NAVAL POSTGRADUATE SCHOOL
Monterey, California

THESIS

MOTION ANALYSIS OF A TROLLEY INTERFACE FOR SHIP-TO-SHIP CARGO TRANSFER

by

Brian Higgins

December 2002

Thesis Advisor: Fotis A. Papoulias

Approved for public release; distribution is unlimited

THIS PAGE INTENTIONALLY LEFT BLANK

REPORT DOCUMENTATION PAGE			Form Approved OMB No. 0704-0188
Public reporting burden for this collection of information is estimated to average 1 hour per response, including the time for reviewing instruction, searching existing data sources, gathering and maintaining the data needed, and completing and reviewing the collection of information. Send comments regarding this burden estimate or any other aspect of this collection of information, including suggestions for reducing this burden, to Washington headquarters Services, Directorate for Information Operations and Reports, 1215 Jefferson Davis Highway, Suite 1204, Arlington, VA 22202-4302, and to the Office of Management and Budget, Paperwork Reduction Project (0704-0188) Washington DC 20503.			
1. AGENCY USE ONLY *(Leave blank)*	**2. REPORT DATE** December 2002	**3. REPORT TYPE AND DATES COVERED** Master's Thesis	
4. TITLE AND SUBTITLE: Motion Analysis of a Trolley Interface for Ship-to-Ship Cargo Transfer			**5. FUNDING NUMBERS**
6. AUTHOR(S) Brian Higgins			
7. PERFORMING ORGANIZATION NAME(S) AND ADDRESS(ES) Naval Postgraduate School Monterey, CA 93943-5000			**8. PERFORMING ORGANIZATION REPORT NUMBER**
9. SPONSORING /MONITORING AGENCY NAME(S) AND ADDRESS(ES) N/A			**10. SPONSORING/MONITORING AGENCY REPORT NUMBER**
11. SUPPLEMENTARY NOTES The views expressed in this thesis are those of the author and do not reflect the official policy or position of the Department of Defense or the U.S. Government.			
12a. DISTRIBUTION / AVAILABILITY STATEMENT Approved for public release; distribution is unlimited			**12b. DISTRIBUTION CODE**

13. ABSTRACT ***(maximum 200 words)***

The goal of this thesis is to investigate the effectiveness of a trolley interface for ship-to-ship cargo transfer. The new interface alleviates some of the torsional problems associated with existing ramp designs and can be effectively utilized for both skin-to-skin and Roll-On Roll-Off operations. A mathematical model is developed in order to predict cargo transfer rates in a seaway. Three dimensional hydrodynamic analysis data are used to calculate expected transfer rates in a seaway between a ship and a discharge facility. Results are presented in standard fully developed Pierson-Moskowitz sea spectra. It is shown that the new design is a viable alternative to existing methods.

14. SUBJECT TERMS Advanced Design Consulting Inc., Hydrodynamic Analysis, Pierson-Moskowitz, Ramp Design, Seabasing, Trolley Interface, WAMIT			**15. NUMBER OF PAGES** 80
			16. PRICE CODE
17. SECURITY CLASSIFICATION OF REPORT Unclassified	**18. SECURITY CLASSIFICATION OF THIS PAGE** Unclassified	**19. SECURITY CLASSIFICATION OF ABSTRACT** Unclassified	**20. LIMITATION OF ABSTRACT** UL

NSN 7540-01-280-5500 Standard Form 298 (Rev. 2-89)
Prescribed by ANSI Std. 239-18

THIS PAGE INTENTIONALLY LEFT BLANK

Approved for public release; distribution is unlimited

MOTION ANALYSIS OF A TROLLEY INTERFACE FOR SHIP-TO-SHIP CARGO TRANSFER

Brian E. Higgins
Lieutenant, United States Coast Guard
B.S., U.S. Coast Guard Academy, 1995

Submitted in partial fulfillment of the
requirements for the degree of

MASTER OF SCIENCE IN MECHANICAL ENGINEERING

from the

NAVAL POSTGRADUATE SCHOOL
December 2002

Author: Brian E. Higgins

Approved by: Fotis A. Papoulias
Thesis Advisor

Young Kwon
Chairman, Department of Mechanical Engineering

THIS PAGE INTENTIONALLY LEFT BLANK

ABSTRACT

The goal of this thesis is to investigate the effectiveness of a trolley interface for ship-to-ship cargo transfer. The new interface alleviates some of the torsional problems associated with existing ramp designs and can be effectively utilized for both skin-to-skin and Roll-On Roll-Off operations. A mathematical model is developed in order to predict cargo transfer rates in a seaway. Three dimensional hydrodynamic analysis data are used to calculate expected transfer rates in a seaway between a ship and a discharge facility. Results are presented in standard fully developed Pierson-Moskowitz sea spectra. It is shown that the new design is a viable alternative to existing methods.

THIS PAGE INTENTIONALLY LEFT BLANK

TABLE OF CONTENTS

THIS PAGE INTENTIONALLY LEFT BLANK

LIST OF FIGURES

THIS PAGE INTENTIONALLY LEFT BLANK

LIST OF TABLES

THIS PAGE INTENTIONALLY LEFT BLANK

ACKNOWLEDGMENTS

I would like to thank the following people for support:

My family for being themselves,

My thesis advisor, Fotis Papoulias, for his patience,

Errol and Kirstin Glenn for the good times,

Jihed Boulares for his help,

Pam Silva for her assistance

And everyone who has helped me here at NPS.

THIS PAGE INTENTIONALLY LEFT BLANK

I. INTRODUCTION

Current United States military doctrine has the US armed forces responding to situations around the globe. One of the most difficult problems facing the US Army and Marine Corps today is how to get large amounts of equipment to a distant battle quickly and safely. Both the Marine Corps and the Army rely on ships to transfer much of their equipment anywhere in the world. Several classes of ships are tasked with this job, they include the LMSR, CAPE-D, CAPE H and CAPE-T designated vessels. These ships transport everything from vehicles, equipment, supplies and ammunition directly to a conflict, where it can either be offloaded to a port, or to a beach in the absence of existing facilities. The Marine Corps also stores hundreds more M-1A1 tanks, LAVs, trucks, HMMWVs and other vehicles aboard Navy ships such as the LHA and LHD, for use during the initial phase of an amphibious assault. Because there is no guarantee that sufficient port facilities will be available at the scene of an attack, these ships must have an alternate method of getting cargo ashore. Ship-to-ship transfer has to be involved in this method, offloading vehicles and equipment onto smaller ships that can take it ashore.

Existing methods for heavy cargo transfer are by means of a ramp interface. The main disadvantage of the existing ramp design is its inability to operate beyond sea state 3. Previous studies have traced this inability to excessive torsional stresses on the ramp for the worst case scenario consisting of two main battle tanks located in the middle of the ramp. This concentrated weight (approximately 140 tons) coupled with the motions at the ramp end points generates stresses that are beyond allowable. This thesis explores a new method of transferring cargo at sea proposed by Advanced Design Consulting, Inc. This new method is based on the use of a trolley-rail interface. Potential advantages of the new interface are (i) reduction in torsional stresses and (ii) reduction in weight.

THIS PAGE INTENTIONALLY LEFT BLANK

II. OVERVIEW OF AMPHIBIOUS WARFARE

As mentioned before, the US military has ships full of military equipment that are prepositioned in friendly ports around the world, where they can be quickly dispatched to a conflict when needed. This concept reduces the response time of the US military to a conflict, and also provides a large sealift capacity that can be quickly used to reinforce Marines who have initiated an amphibious operation. After Marines have secured a section of beach, these prepositioned ships drive up to within 2 NM of the beach, and offload their entire cargo either via existing port facilities, or directly onto the beach. This buildup of equipment and supplies ashore is what some refer to as the "iron mountain." As the equipment and supplies are being taken ashore, Marines are flown into the region, and meet up with their equipment on the beach. Once the appropriate combat gear has been chosen, based on the threat and the area of operation, the offensive can be resumed.

There are problems associated with this method of operation. This type of operation is predictable because few beaches are able to support such an amphibious attack. Deep draft vessels must be able to get within 2 nautical miles of the coastline to offload, and access to an airport is important. The beach also has to be somewhat sheltered, because offloading can only be done in conditions up to sea state 3. Large cargo, such as a 48,000 lb container of ammunition or a 135,000 lb M-1A1 tank [Ref 2], is only able to be transferred by ramp or crane. The current ramps experience high torsional stress when they are heavily loaded and then twisted by wave action. Crane loads will swing when the ship is moved by wave action. Another problem lies in the delay associated with offloading. As all of the equipment is brought ashore, the Marines must cease major offensive operations and defend the "iron mountain." This pause is frequently referred to as an "operational pause," and can last for several days. A third problem lies in the fact that the "iron mountain" is a large immobile target that needs to be defended. The Marine Corps has recognized these and other problems, and their solution is to change existing amphibious warfare tactics. The two concepts under consideration that promise to have the greatest impact on how U.S. Amphibious warfare is conducted are STOM (Ship To Objective Maneuver) and Seabasing [Ref 4]. STOM

involves a direct attack on the objective, without any buildup of supplies on the shore. In STOM, Navy ships are used as a staging ground, eliminating the need to create a staging ground ashore. No operational pause is needed. Using Navy ships as a base of operations is called "Seabasing."

There are several ramifications associated with the implementation of these new concepts. If Seabasing is done, the requirements for ship-to-shore and ship-to-ship transfer change. Seabasing will allow amphibious ships to remain further offshore, up to 250 nautical miles from the beach, where the average sea states are much higher. Therefore, more emphasis will be placed on the ability to conduct operations in higher sea states. As mentioned earlier, current at-sea cargo transfer systems are not able to safely operate in conditions above sea state 3.

The Trolley-Rail system proposed by Advanced Design Consulting, Inc. represents a new method for transferring cargo between ships in higher sea states. The preliminary design drawings indicate that the system is composed of a trolley with two beams, or bridging structures. The two bridging structures act as rails of a track, laid between the two ships, and the trolley travels back and forth between the two ships along the rails. One side of the trolley has a series of rollers along the trolley edge. These rollers run along a track in the rail. The other side of the trolley is supported by a pivot, making the two bridging structures independent and eliminating much of the ramp end torsional loading. A basic schematic of the system is shown in Figure (1):

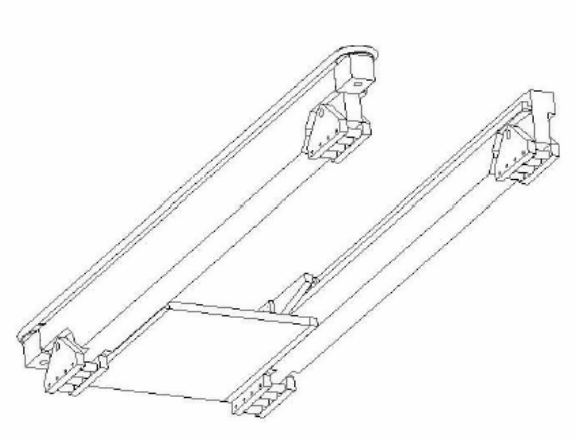

Figure 1. Trolley-Rail System

An electric motor uses a cable-pulley system to pull the trolley up and down the rails. This thesis investigates the motions that this trolley-rail transfer system could encounter during operations in various sea states, and provides a rough model to determine an expected transfer rate for this device. This rate can then be compared with the rates of systems that are used today for at-sea cargo transfer. First, a model is constructed that determines how 2 ships in close proximity react to a variety of sea states, so that data describing their motion and the relative motion between them is created.

THIS PAGE INTENTIONALLY LEFT BLANK

III. MODELING

A. PHYSICAL MODELING

When computing the seakeeping of a vessel, a ship model is required. In the case of this study, two ship models are required so that ship-to-ship transfer can be analyzed. The ship modeling is based on the RRDF 2000 (Roll-On Roll-Off Discharge Facility) and the Cape-D class of ships, both of which are currently in service with the Marine Corps' for use in transport and transfer of cargo and vehicles at sea during an amphibious operation. Although raw modeling data for these two vessels is used because it was available, different ship models can also be easily accommodated. For demonstration purposes, the analysis focuses on these two vessels.

The RRDF is made up of a number of interconnected modules, in an asymmetrical way, as can be seen in Figure (2):

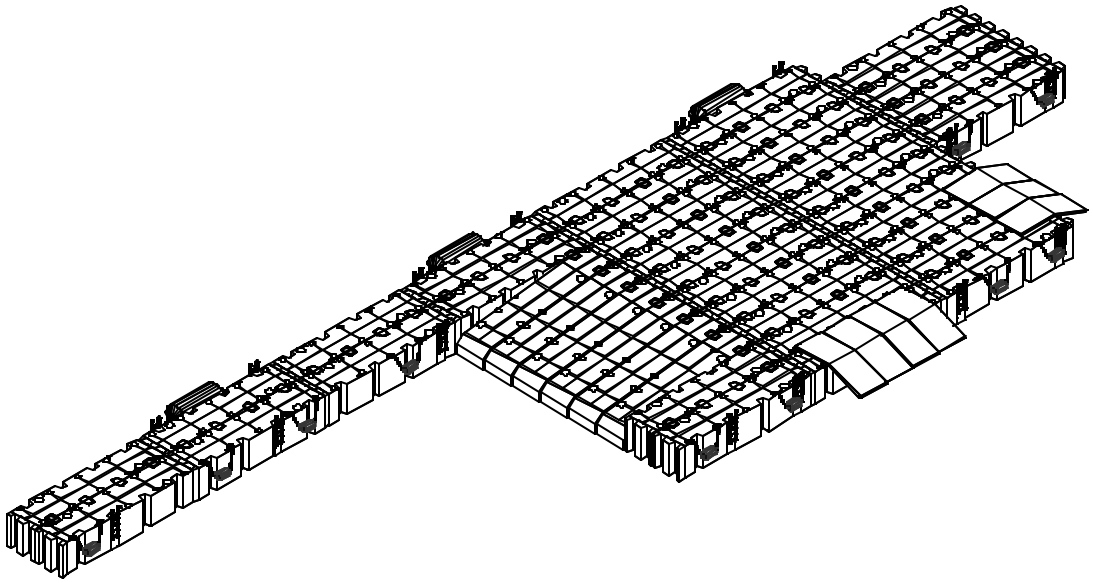

Figure 2. An isometric view of the RRDF

Each module has 8x8x40 ft nominal dimensions, and floats at an approximate draft of 2 ft. The RRDF is placed 100 ft astern of the Cape-D ship, which is equipped with a stern ramp only.

The Cape-D ship has a length of 634 ft, beam 97 ft, nominal draft 32.4 ft, and displaces approximately 36,000 tons. This ship is part of the Ready Reserve Force and is one of the main ships used for dry cargo transfer by the Military Sealift Command's (MSC) Strategic Sealift Forces. Typical views of the ship are shown in Figure (3).

Figure 3. Typical Views of the Cape D Ship Class

B. HYDRODYNAMIC MODELING

Once a 3-dimensional model of the ship had been obtained, it was placed into a 'virtual seaway.' Modern seakeeping computations are used in all aspects of the engineering of the marine environment. Reference 5 describes the developmental history of ship motion analysis in detail, beginning with the original work done by Froude on ship rolling. Computations can be performed using a variety of techniques- from simple strip theory to extremely complicated fully nonlinear unsteady Reynolds Averaged Navier-Stokes equations in the time domain. The computer program WAMIT is used to create hydrodynamic modeling data for this report.

WAMIT, short for Wave Analysis MIT, was first used in 1988. The offshore oil industry wanted to model hydrodynamic motion of vessels, and strip theory would not work for the vessel geometry that is typically used in the exploration and production of offshore gas and oil. WAMIT is based on the panel method for analyzing hydrodynamic interaction (radiation and diffraction) with floating or submerged bodies. WAMIT is now widely recognized as a highly accurate and efficient program for analyzing wave interactions with complex structures and vessels.

As described by the creators of WAMIT [Ref 6], the basic underlying theme of the program lies in the linear frequency-domain potential representation of the fluid motion. WAMIT evaluates the unsteady hydrodynamic pressure, loads and motions of the body, as well as the induced pressure and velocity in the fluid domain. Free-surface and body-boundary conditions are linearized, and the flow is assumed to be potential, free of separation or lifting effects.

WAMIT utilizes the panel method for discreetization, allowing for numerical solutions of the integral theorems of the Green function. The mean position of the body's wetted surface area is approximated by a collection of quadrilaterals. Four vertices, lying on the body's surface, define each quadrilateral. In general the quadrilaterals defined above are not plane, but if a sufficiently fine discreetization is used for the boundary surface with continuous curvature, each element will approach a plane surface.

Assuming low speed flow and neglecting the viscous effects allows the use of potential flow theory. Low speed flow is irrotational ($\Delta \times V = 0$), and so the velocity potential Φ exists such that:

$$\frac{d\Phi}{dx} + \frac{d\Phi}{dy} + \frac{d\Phi}{dz} = 0 \tag{1}$$

The continuity equation reduces to the Laplace equation:

$$\frac{d^2\Phi}{dx^2} + \frac{d^2\Phi}{dy^2} + \frac{d^2\Phi}{dz^2} = 0 \tag{2}$$

Since any potential flow can be solved using complex variables, and based on the fact that the waves are harmonic in nature, a complex velocity potential f can be defined where F = $Real(j\, e^{iwt})$. Here, ? = the frequency of the incident wave and t = time. Because it is assumed that there is a free surface condition, the linearized form of the free surface condition is:

$$j_z - Kj = 0 \quad \text{and} \quad z = 0 \tag{3}$$

where $K = \frac{w^2}{g}$, and g is the acceleration of gravity. f, the velocity potential, is then broken up into radiation and diffraction components:

$$j = j_R + j_D \tag{4}$$

On the undisturbed position of the body boundary, the radiation and diffraction potentials are subject to the conditions:

$$j_{jn} = n_j \tag{5}$$

$$j_{Dn} = 0 \tag{6}$$

where $(n_1, n_2, n_3) = n$ and $(n_4, n_5, n_6) = x \times n$, $x = (x, y, z)$. The unit vector n is normal to the body boundary and points out of the fluid domain.

The radiation and diffraction components of the velocity potential (f) were solved with integral equations that were derived using Green's Theorem. For radiation, the

integral equation satisfied by the radiation velocity potentials f_j on the body boundary is of the form:

$$2p\,j_j(x) + \iint_{S_b} j_j(x)\frac{\partial G(x;x)}{\partial n_x}dx = \iint_{S_b} n_j G(x;x)dx \tag{7}$$

where S_b denotes body wetted surface at calm water. The equation for total diffraction velocity potential f_D is of the form:

$$2p\,j_D(x) + \iint_{S_b} j_D(x)\frac{\partial G(x;x)}{\partial n_x}dx = 4p\,j_0(x) \tag{8}$$

By doing this, WAMIT incorporates hydrodynamic interaction effects between floating bodies and, therefore, properly accounts for wave diffraction by each individual body. In the context of ship motions, this means that the six degree of freedom motions for each body are coupled together. Therefore, the resulting added-mass and damping matrices are 12x12 as opposed to 6x6 for a single body. The two 6x6 off-diagonal block matrices represent acceleration and velocity coupling between the two bodies. Although the coupling terms from the RRDF to Cape-D are small and can be neglected, they have been retained in the calculations since the additional computational burden is small. Coupling from Cape-D to RRDF is significant and cannot be neglected. The hydrostatic restoring matrix for the two bodies is also a 12x12 matrix. This is comprised of the two 6x6 matrices of the individual bodies. The reason for this is that in an unbounded fluid domain, there is no hydrostatic coupling between adjacent floating bodies.

Initial calculations are based on the equations of motion for the two floating bodies in the frequency domain. Following standard seakeeping notation, these equations are written as:

$$\sum_{j=1}^{12}\left[-w^2\left(M_{ij} + A_{ij}(w)\right) + iwB_{ij}(w) + C_{ij}\right]x_j = X_i, \tag{9}$$

where M_{ij} is the inertia matrix, $A_{ij}(w)$ is the added mass matrix, $B_{ij}(w)$ is the wave damping matrix, C_{ij} is the hydrostatically derived restoring matrix, x_j is the complex body amplitude of motion, and X_i is the wave exciting force or moment.

The added mass and damping coefficients are calculated by a surface integration of the velocity potential

$$A_{ij} - \frac{i}{w} B_{ij} = r \iint_{S_b} n_i f_j \, dS \tag{10}$$

Exciting forces are calculated from direct integration of the hydrodynamic pressure on the body, the hydrostatic matrix elements are calculated from integrations of the static pressure distribution on the body, and the mass matrix consists of the standard 6x6 inertia matrix for each of the two rigid bodies:

$$M = \begin{pmatrix} m & 0 & 0 & 0 & mzg & -myg \\ 0 & m & 0 & -mzg & 0 & mxg \\ 0 & 0 & m & myg & -mxg & 0 \\ 0 & -mzg & myg & I11 & I12 & I13 \\ mzg & 0 & -mxg & I21 & I22 & I23 \\ -myg & mxg & 0 & I31 & I32 & I33 \end{pmatrix} \tag{11}$$

More detailed information about the theory behind WAMIT can be found in Reference (6).

WAMIT calculations used for this report are performed for wave frequencies ranging from 0.3 to 2.5 rad/sec to cover the range of sea spectra energy. 24 wave headings relative to ship heading are used, from 0 to 345 degrees in 15 degree increments. 0 degrees correspond to following (astern) seas, 180 degrees to head seas, 90 degrees to starboard beam seas, and 270 degrees to port beam seas. Both bodies are at zero forward speed.

C. ENVIRONMENTAL MODELING

Following the frequency response calculations outlined in the previous section, the motions of the two bodies are calculated in a realistic seaway. The environment at which the bodies are operating is modeled as a random process. Two sea spectrum

representations are used for the calculations: The Pierson-Moskowitz spectrum and the Bretschneider spectrum.

The Pierce-Moskowitz spectrum is used for the calculations. The Pierson-Moskowitz spectrum was developed by the offshore oil industry to model fully developed waves in the North Sea [Ref 7]. It is a single parameter spectrum based either on wind speed or the significant wave height. This corresponds to fully-developed unidirectional seas. The semi-empirical formulation of the Pierson-Moskowitz spectrum is

$$S(w) = \frac{a\,g^2}{w^5} \exp\left[-b\left(\frac{g}{Uw}\right)^4\right], \tag{12}$$

where the coefficients are $a = 8.1\times10^{-3}$ and $b = 0.74$. U is the wind velocity at a standard height of 19.5 meters above the free surface, and g is the acceleration of gravity. Typical properties of the spectrum are as shown in Figure (4).

PIERSON-MOSKOWITZ SEA SPECTRUM							
Sea State	Significant Wave (Ft)	Significant Range of Periods (Sec)	Period of Maximum Energy (Sec)	Frequency Maximum Energy (Sec)	Average Period (Sec)	Average Wave Length (Ft)	Wind Speed (Kts)
0	0.10	0.34 - 1.09	0.87	7.22	0.62	1.31	2.51
0	0.15	0.42 - 1.33	1.07	5.87	0.76	1.97	2.83
1	0.50	0.77 - 2.43	1.95	3.22	1.39	0.57	5.17
1	1.00	1.09 - 3.43	2.75	2.28	1.96	13.14	7.31
1	1.20	1.19 - 3.76	3.02	2.08	2.15	15.76	8.01
2	1.50	1.34 - 4.21	3.38	1.86	2.40	19.70	5.05
2	2.00	1.54 - 4.86	3.90	1.61	2.77	26.27	10.34
2	2.50	1.72 - 5.43	4.36	1.44	3.10	32.84	11.36
2	3.00	1.89 - 5.95	4.78	1.31	3.40	39.41	12.66
3	3.50	2.04 - 6.43	5.16	1.22	3.67	45.98	13.68
3	4.00	2.18 - 6.87	5.52	1.14	3.92	52.54	14.62
3	4.50	2.31 - 7.29	5.86	1.07	4.16	59.11	15.51
3	5.00	2.44 - 7.68	6.17	1.02	4.38	65.68	16.35
4	6.00	2.67 - 8.41	6.76	0.93	4.80	78.82	17.91
4	7.00	2.89 - 9.09	7.30	0.86	5.19	91.95	19.34
4	7.50	2.99 - 9.41	7.56	0.83	5.37	98.52	20.02
5	8.00	3.08 - 9.71	7.81	0.80	5.55	105.09	20.68
5	9.00	3.27 - 10.30	8.28	0.76	5.88	118.22	21.93
5	10.00	3.45 - 10.86	8.73	0.72	6.20	131.36	23.12
5	12.00	3.78 - 11.90	9.56	0.66	6.79	157.63	25.33
6	14.00	4.08 - 12.85	10.33	0.61	7.34	183.90	27.36
6	16.00	4.36 - 13.74	11.04	0.57	7.84	210.17	29.24
6	18.00	4.63 - 14.57	11.71	0.54	8.32	236.45	31.02
6	20.00	4.88 - 15.36	12.34	0.51	8.77	262.72	32.70
7	25.00	4.45 - 17.17	13.80	0.46	9.80	328.40	36.56
7	30.00	5.97 - 18.81	15.12	0.42	10.74	394.08	40.04
7	35.00	5.45 - 20.32	16.33	0.38	11.60	459.76	43.25
7	40.00	6.90 - 21.72	17.46	0.36	12.40	525.43	46.24
8	45.00	7.32 - 23.04	18.52	0.34	13.15	591.11	49.04
8	50.00	7.71 - 24.28	19.52	0.32	13.87	656.79	51.70
8	55.00	8.09 - 25.47	20.47	0.31	14.54	722.47	54.22
8	60.00	8.45 - 26.60	21.38	0.29	15.19	788.15	56.63
9	70.00	9.12 - 28.73	23.09	0.27	16.41	919.91	61.17
9	80.00	9.75 - 30.72	24.69	0.25	17.54	1098.87	65.39
9	90.00	10.35 - 32.68	26.19	0.24	18.60	1182.23	69.36
9	100.00	10.91 - 34.34	27.60	0.23	19.61	1313.59	73.11

Figure 4. Pierson-Moskowitz Sea Spectrum

The Bretschneider spectrum is used to give a more realistic seaway estimation. The semi-empirical formulation of the Bretschneider spectrum is:

$$S(w) = \frac{1.25}{4}\frac{w_m^4}{w^5}U^2 e^{-1.25\left(\frac{w_m}{w}\right)^4} \qquad (13)$$

The Bretschnieder spectrum is a two-parameter wave spectrum, improving on the Pierson-Moskowitz spectrum. It is based on either wind speed or significant wave height, and also the wave frequency. Again, it only represents fully developed seas. Developing seas have a broader spectral peak, and decaying seas have a narrower peak.

III. RESULTS

Results are obtained for the cases modeled above, with the RRDF placed 100 feet astern of the Cape-D ship. As mentioned before, this was done in order to be consistent with the current version of the ship, which is equipped with a stern ramp. For demonstration purposes, a trolley length of 100 ft was assumed. All results are obtained for significant wave heights ranging from 0 to 30 ft. A significant wave height of 30 ft corresponds to Sea State 7, while Sea State 5 is for a significant wave height of about 10 ft. The results are presented in standard polar plots, where the radial coordinate is the significant wave height (in feet) and the angular coordinate is the wave heading (in degrees). The color scale represents the value in the figure caption, with the units indicated. All motions, velocities, and accelerations are in terms of their RMS (root mean square) values. To get significant single amplitudes, the RMS values need to be multiplied by 2, for an approximate 8-hour maximum amplitude they should be multiplied by 4. The results are categorized in the following subsections.

A. BODY MOTIONS

Figures (5) through (14) show the motions of the Cape-D and the RRDF. It can be seen that Cape-D response is port/starboard symmetric, indicating the minimal influence of the RRDF on the motion of the ship. On the other hand, there is some asymmetry in the RRDF response. This is due to the slight asymmetric placement of the RRDF astern of the ship, and also due to the asymmetric nature of the RRDF. Linear motions are in RMS feet, while angular motions are in RMS radians. We can see that:

- Heave motion for the Cape-D is much smaller that RRDF heave. The RRDF is essentially following the total wave motion. This is because the Cape-D is much heavier than the RRDF, and so the Cape-D will not be as affected by the wave motion. The Heave of the RRDF was expected to nearly equal the height of the seas, but at times the model shows it exceeding the height of the seas, which is most likely due to modeling difficulty in WAMIT.

- RRDF pitch and roll are much smaller than that of the ship. This is due to the very large stiffness (metacentric height) of the RRDF in both roll and pitch.
- Both sway and yaw motions of the RRDF exceed the corresponding motions for the Cape-D.

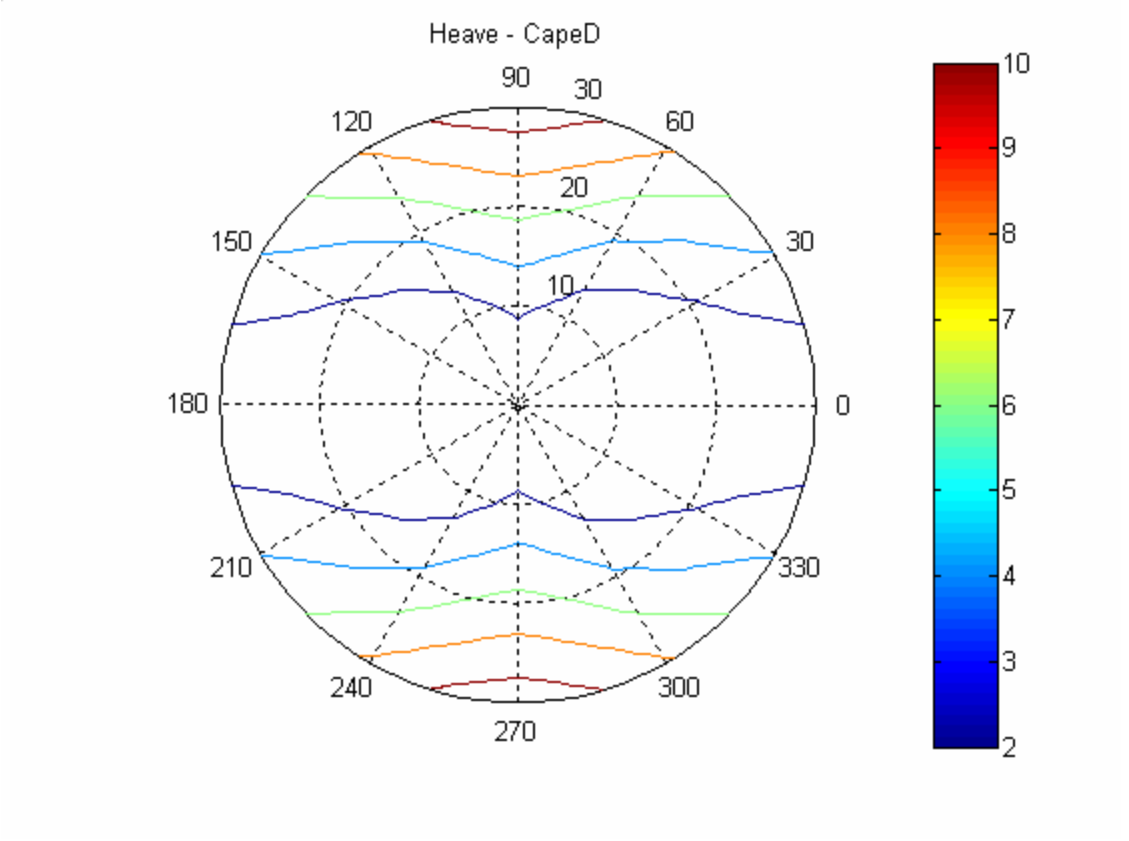

Figure 5. Heave Motion (feet), Cape-D

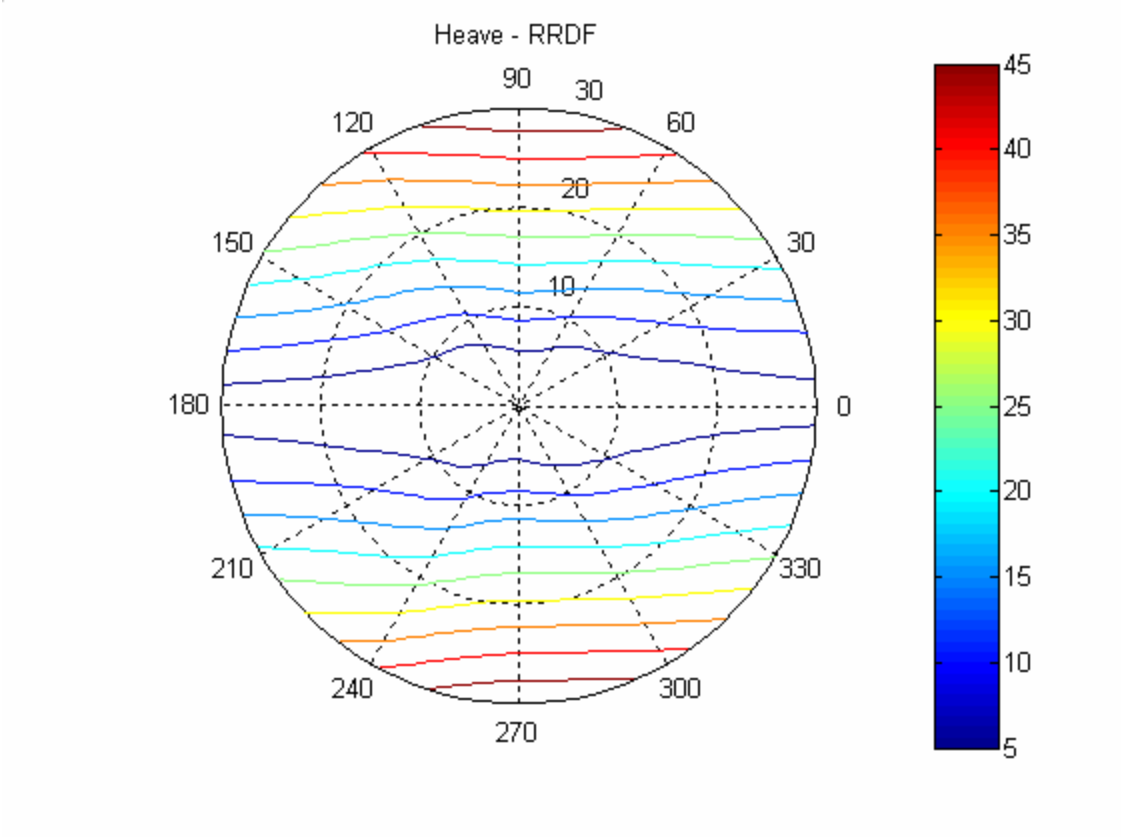

Figure 6. Heave Motion (feet), RRDF

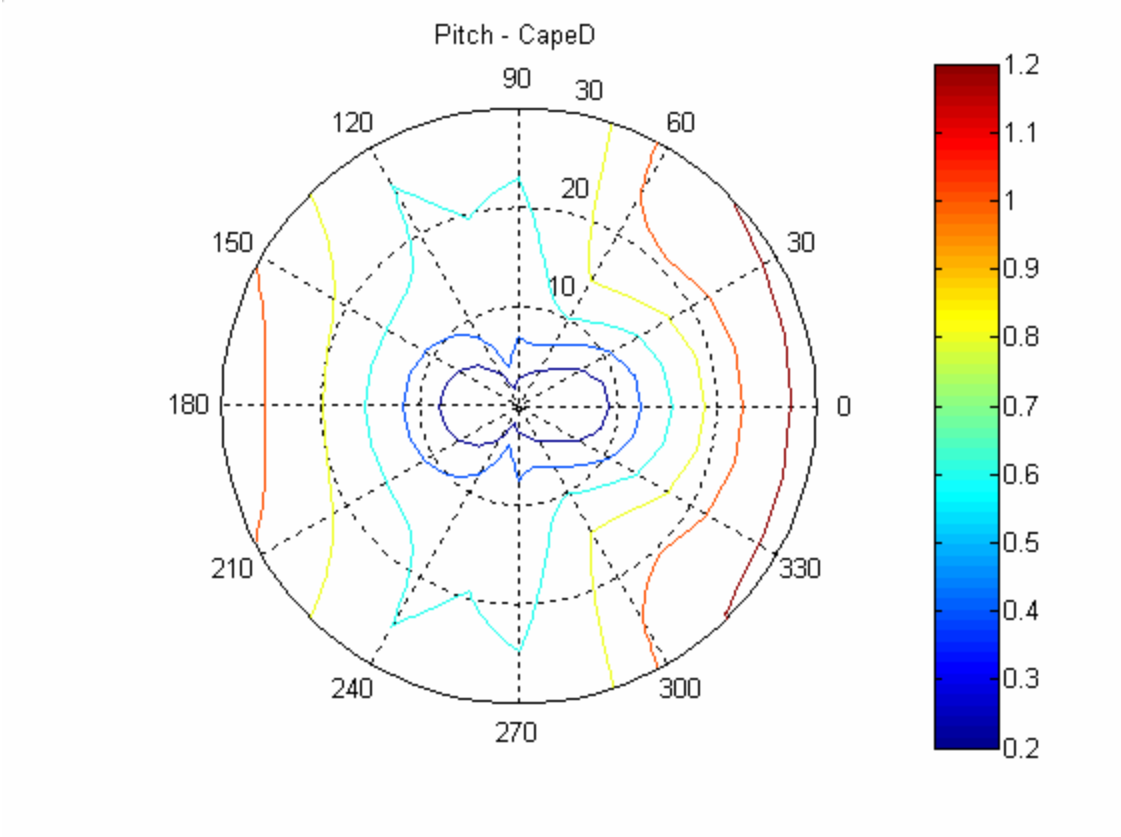

Figure 7. Pitch Motion (degrees), Cape-D

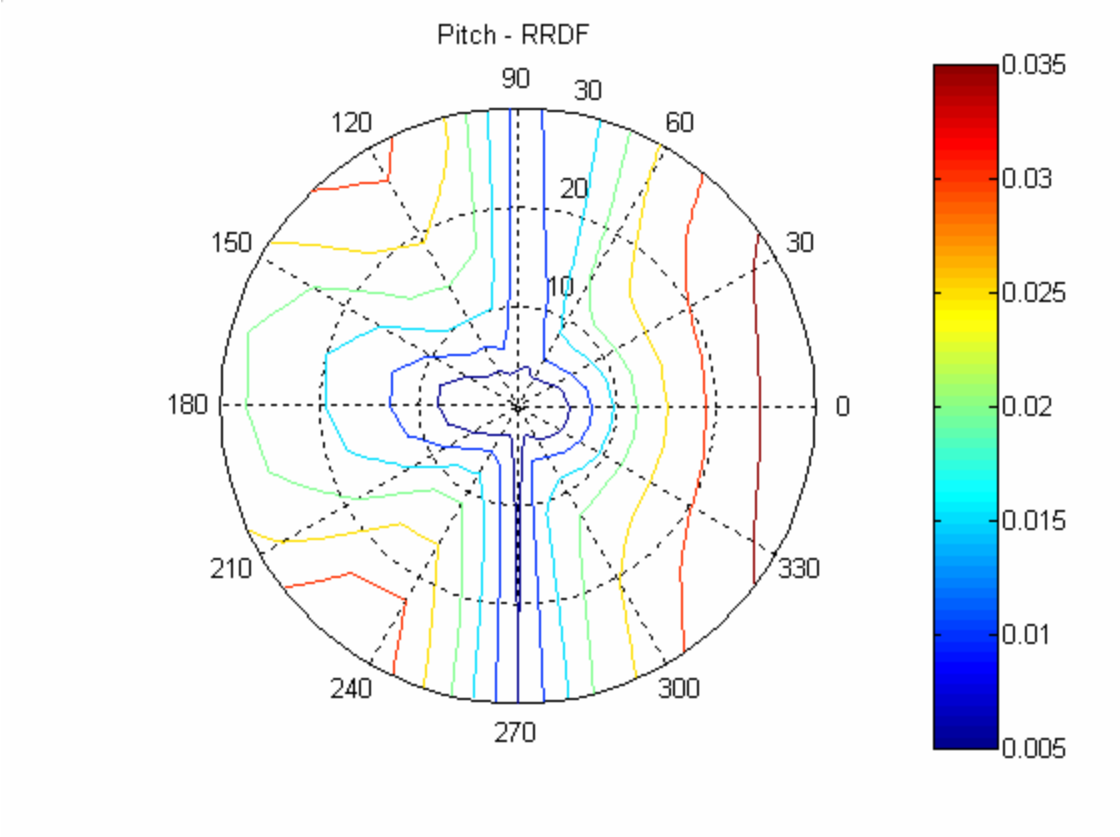

Figure 8. Pitch Motion (degrees), RRDF

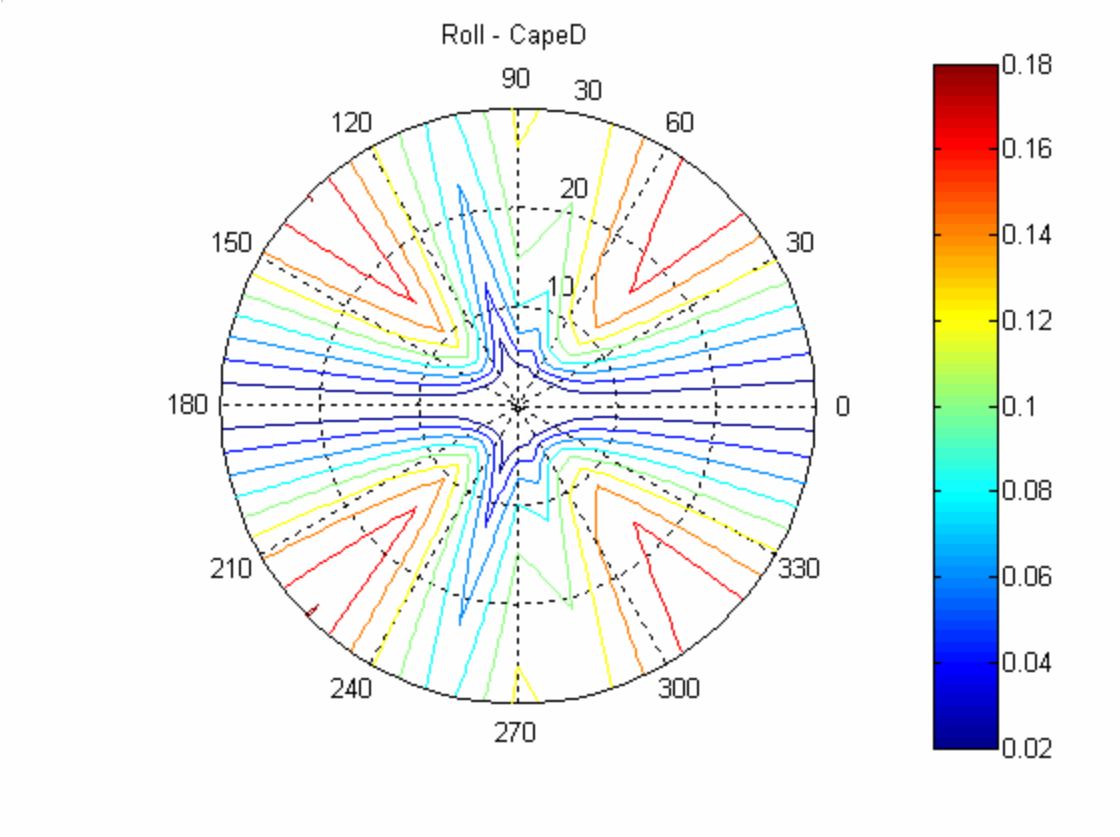

Figure 9. Roll Motion (degrees), Cape-D

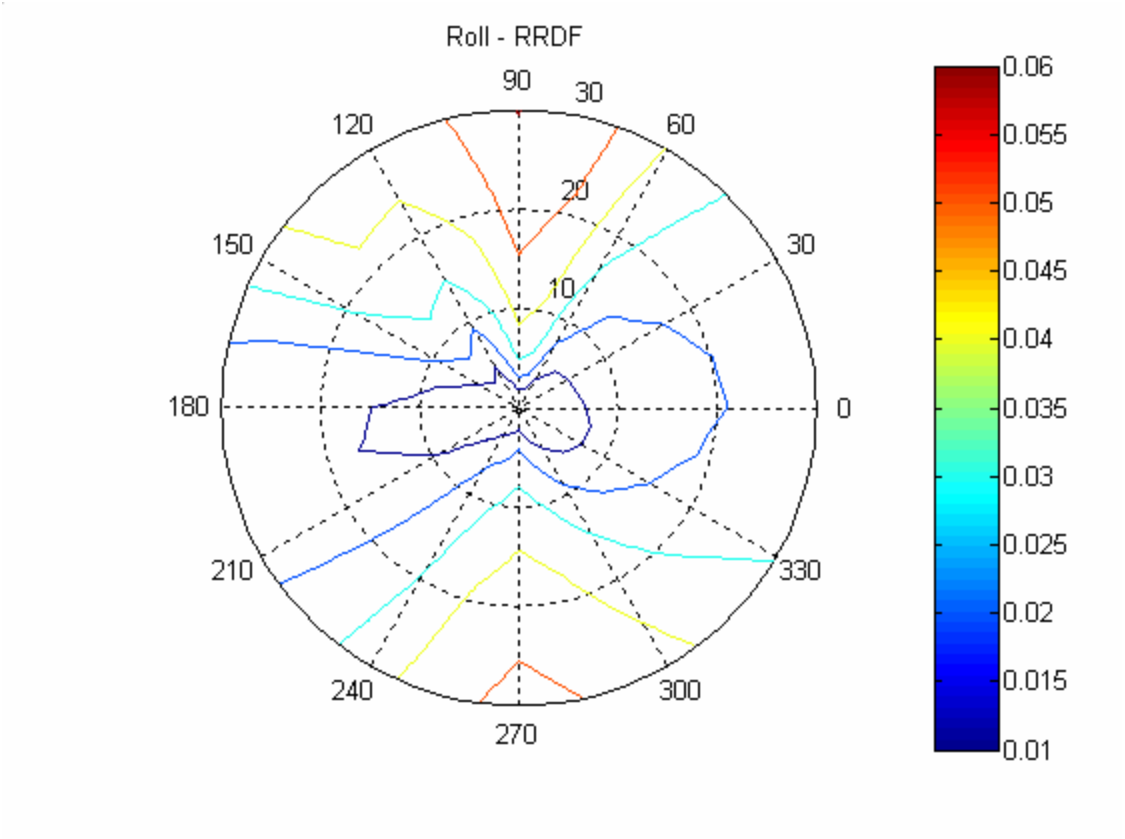

Figure 10. Roll Motion (degrees), RRDF

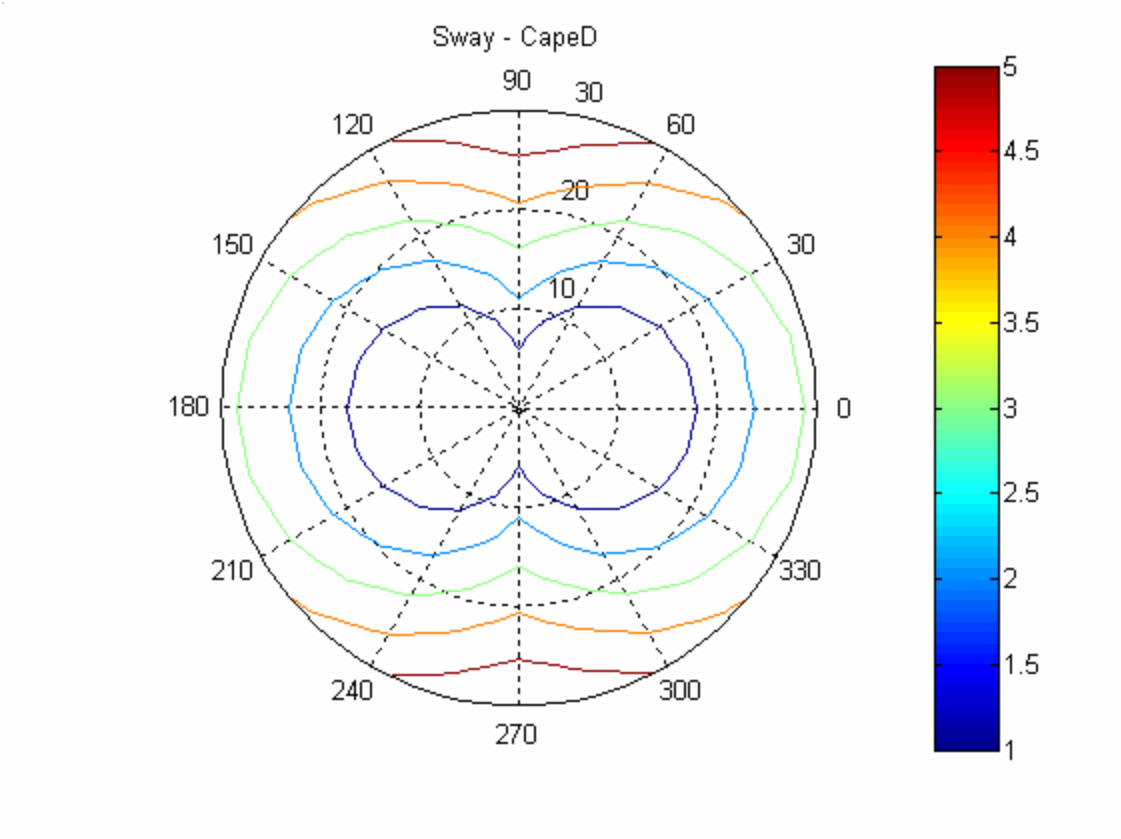

Figure 11. Sway Motion (feet), Cape-D

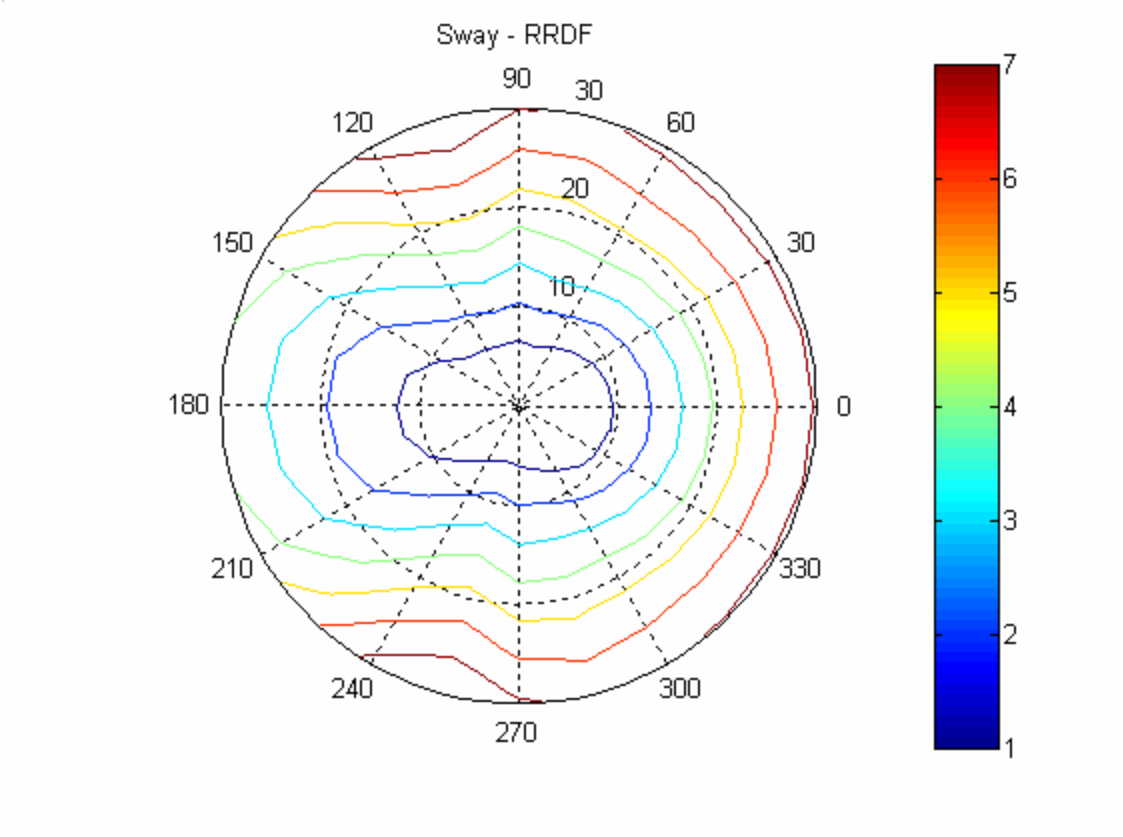

Figure 12. Sway Motion (feet) - RRDF

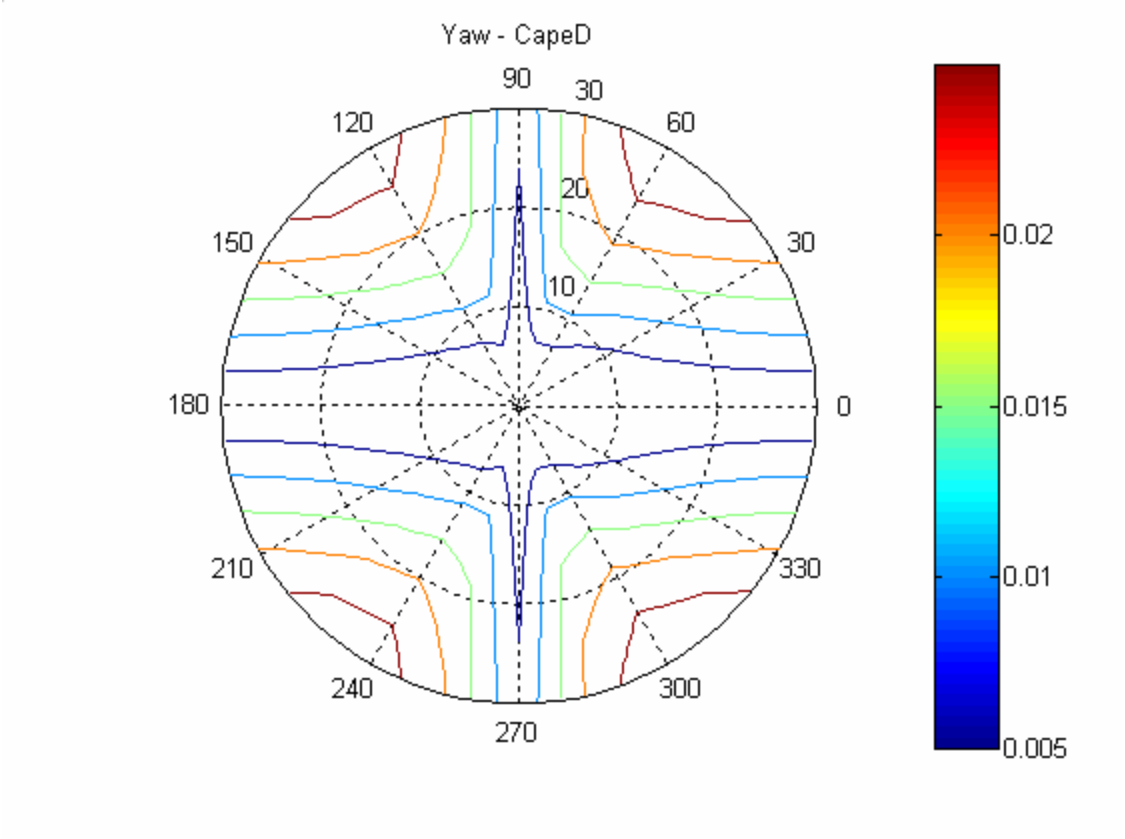

Figure 13. Yaw Motion (degrees), Cape-D

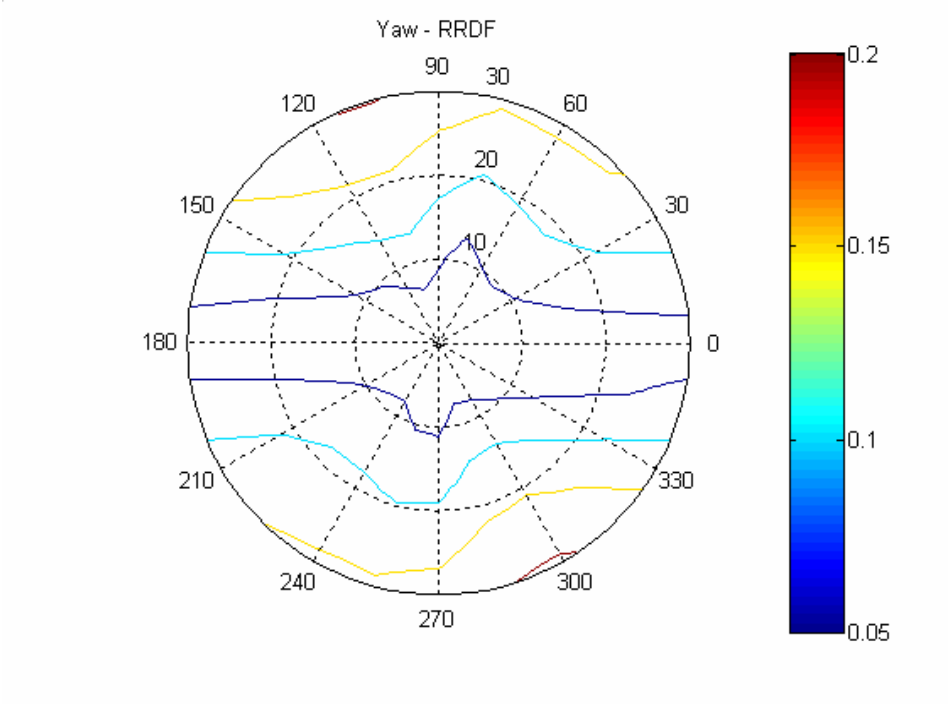

Figure 14. Yaw Motion (degrees) – RRDF

B. TROLLEY MOTIONS, VELOCITIES AND ACCELERATIONS

Figures (15) through (20) present the vertical motions, velocities, and accelerations at the trolley ends, both on the RRDF and the Cape-D side. Vertical motions are calculated by superposition of the heave, pitch, and roll motions for each point at the assumed location of the trolley, either at the Cape-D side or the RRDF side. In the results that follow, motions are in feet, velocities in ft/sec, and accelerations in g's (32.2 ft/s^2). In all cases, motions are higher at the RRDF side. For the case of a ship-to-ship skin-to-skin replenishment, the corresponding values of the response are expected to be similar to those at the Cape-D side Maximum vertical trolley motion at sea state 5 is approximately 16 ft RMS, velocity is about 11 ft/sec RMS, and acceleration 0.25 g's. This maximum occurs consistently in beam seas, as can be seen in the figure. The corresponding values for the Cape-D side are of course smaller, while maximum occurs at fore- and aft-quartering seas.

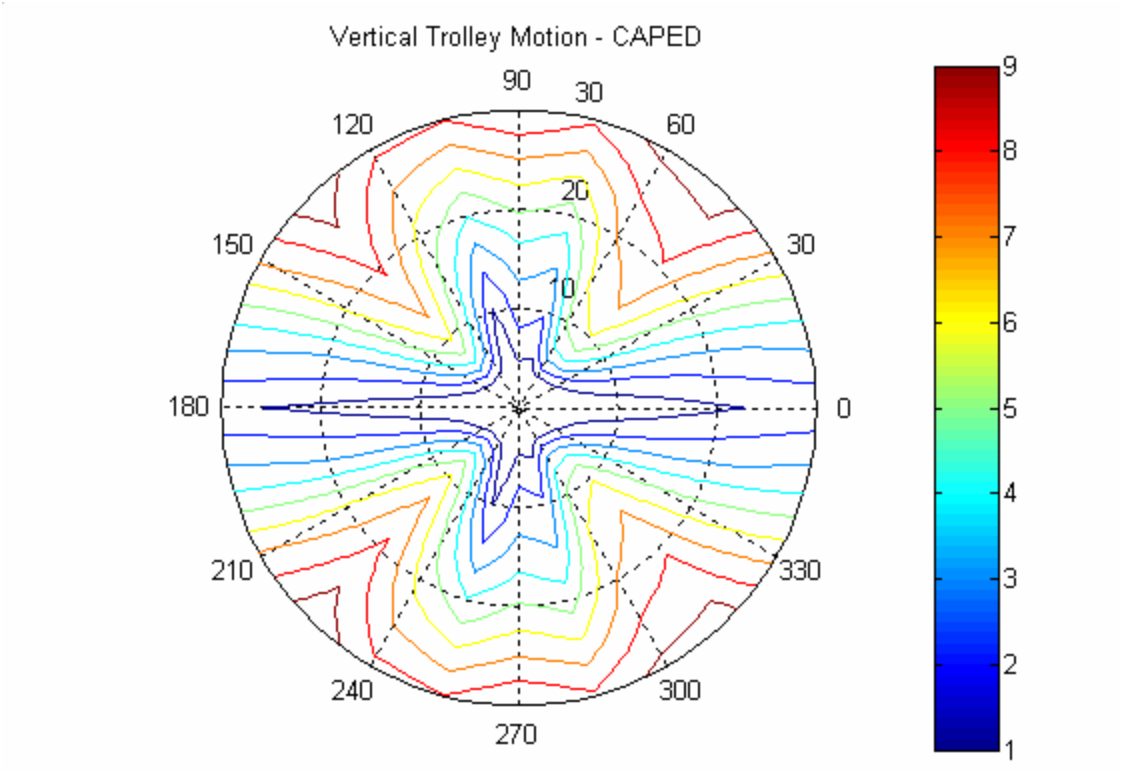

Figure 15. Vertical Trolley Motion (feet), Cape-D

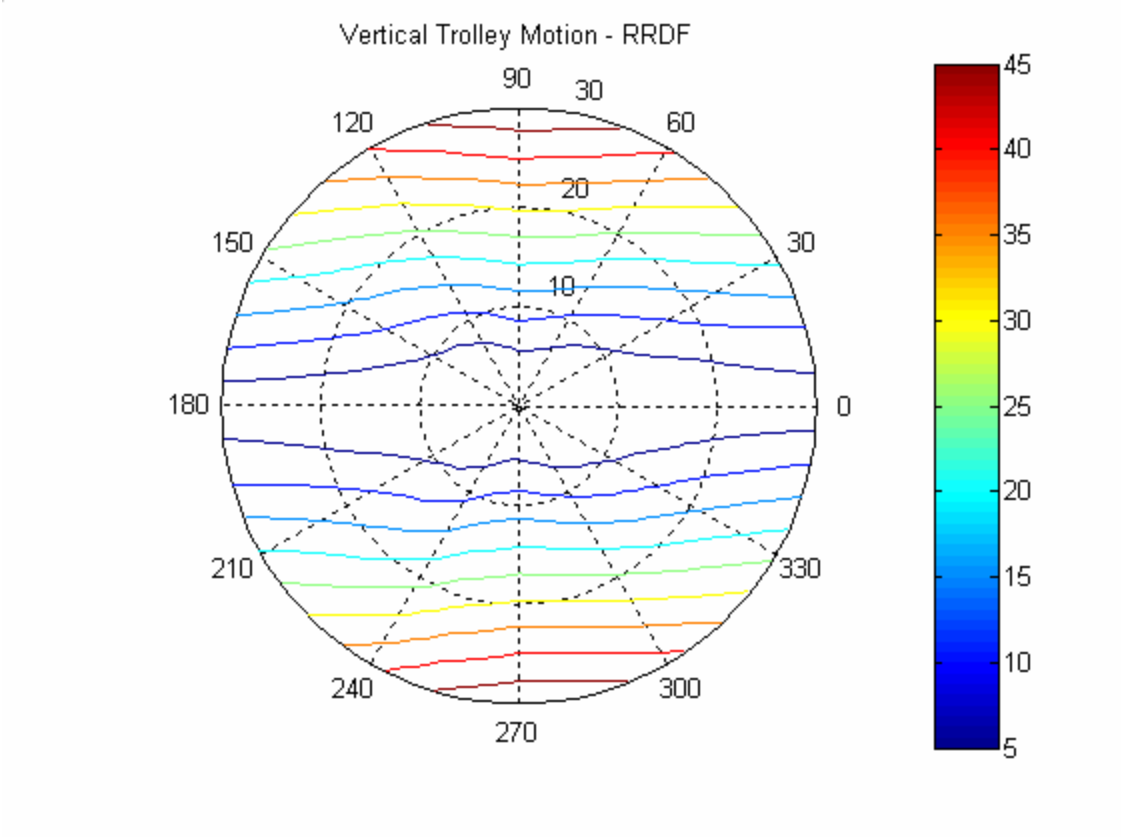

Figure 16. Vertical Trolley Motion (feet) - RRDF

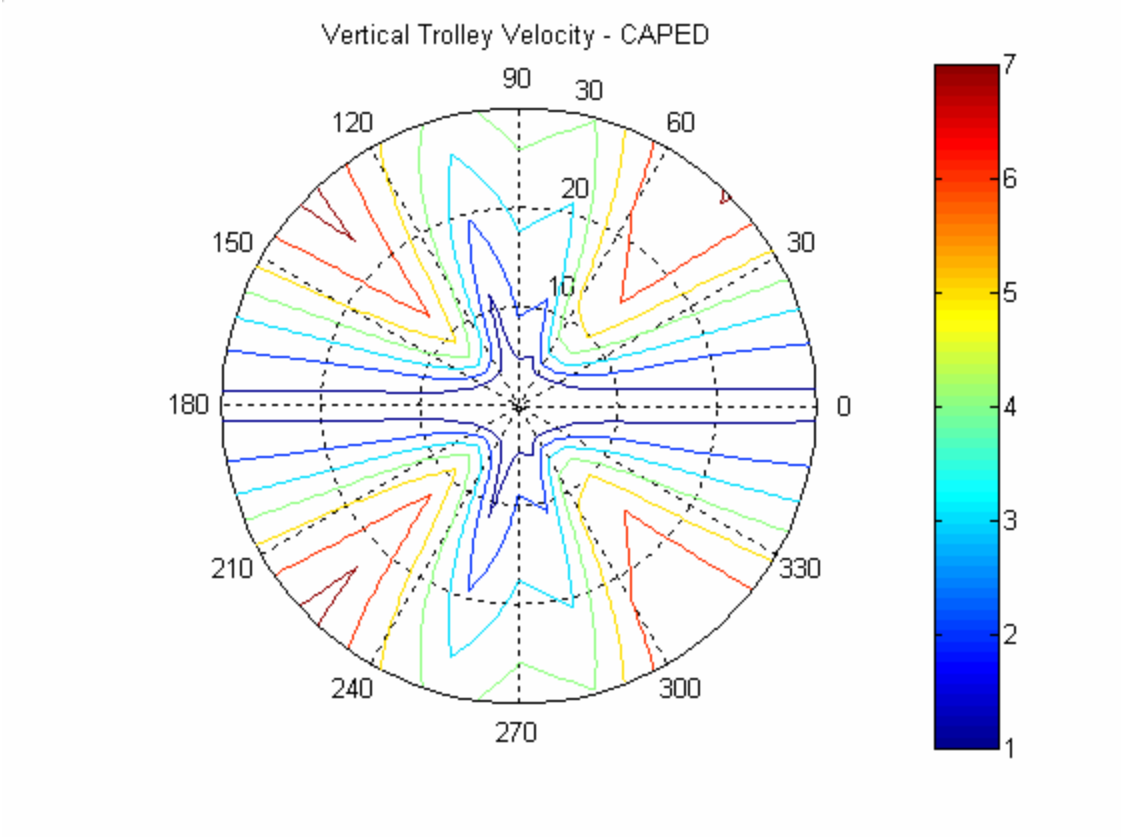

Figure 17. Vertical Trolley Velocity (feet/second), Cape-D

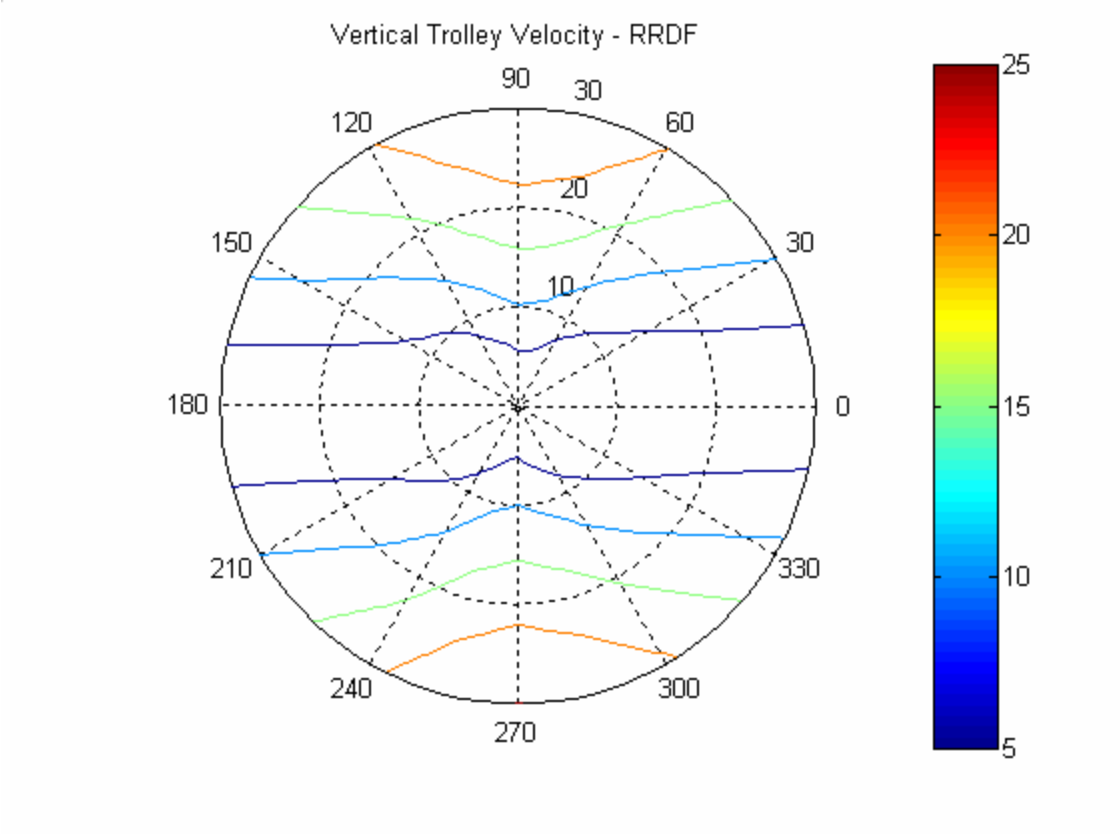

Figure 18. Vertical Trolley Velocity (feet/second), RRDF

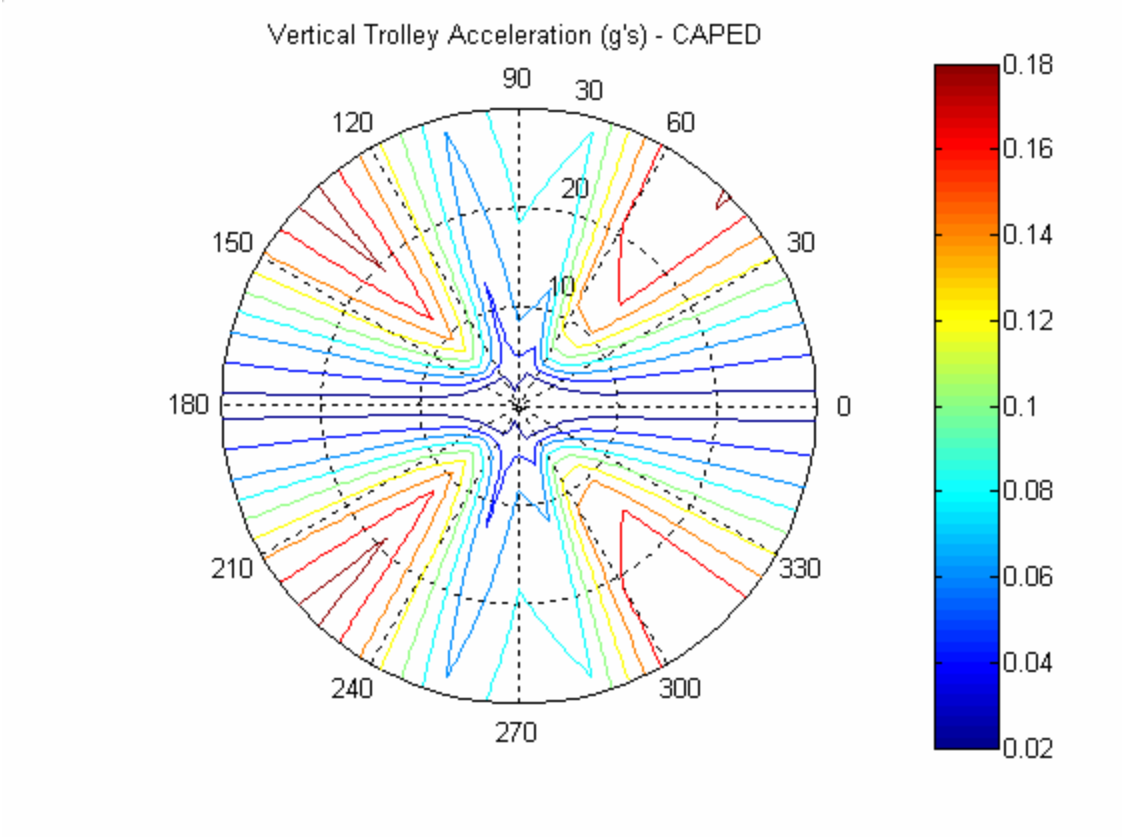

Figure 19. Vertical Trolley Acceleration(g's), Cape-D

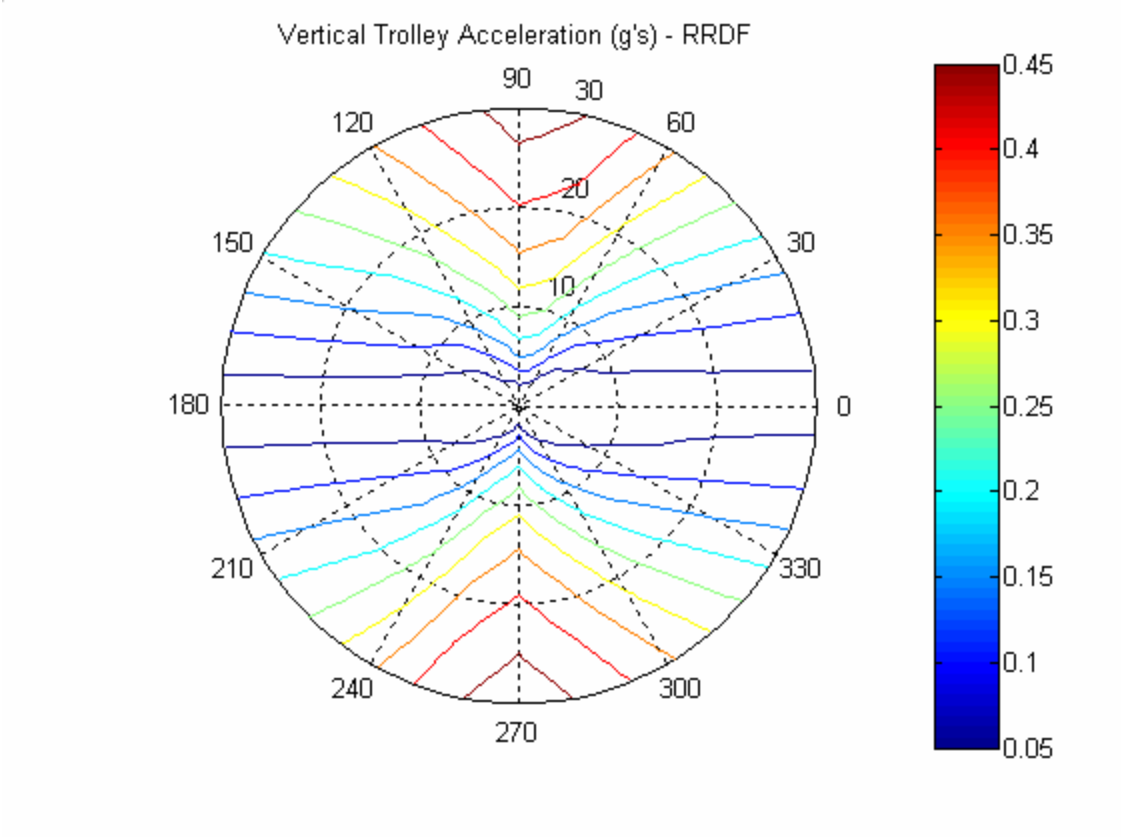

Figure 20. Vertical Trolley Acceleration (g's), RRDF

C. RELATIVE MOTIONS

Figures (21) through (26) show the results for the relative motions, velocities and accelerations of the trolley between the Cape-D and the RRDF ends. Relative motions are calculated by taking into consideration the magnitude as well as the phase angle between the motions at the two end points. There is some asymmetry between port and starboard seas due to the RRDF geometric asymmetry and the hydrodynamic interactions between the two bodies as explained previously. Maximum RMS value of the trolley vertical angle ("pitch") is about 8 degrees for beam seas. Maximum RMS vertical angular velocity is about 5 deg/sec, and maximum RMS angular acceleration is also about 5 deg/sec^2. The corresponding values for horizontal motion, velocity, and acceleration are 7 ft, 4.5 ft/sec, and 0.12 g's, respectively. It should be mentioned that horizontal motions correspond to the relative motion between the two trolley touch-down points; the trolley is assumed to be simply resting on the two bodies and can slide in-and-out freely.

Therefore, the above numbers can be used in order to provide estimates for the necessary safety overheads during the trolley design phase.

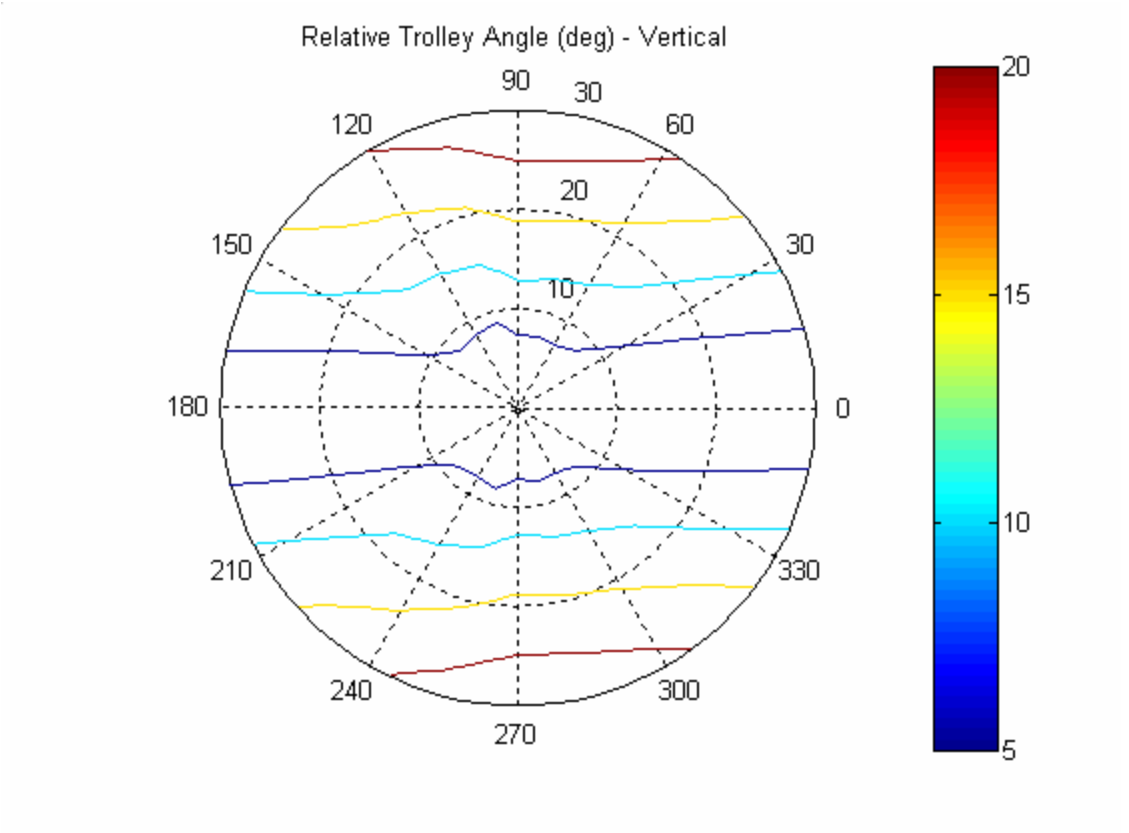

Figure 21. Relative Vertical Trolley Angle (degrees)

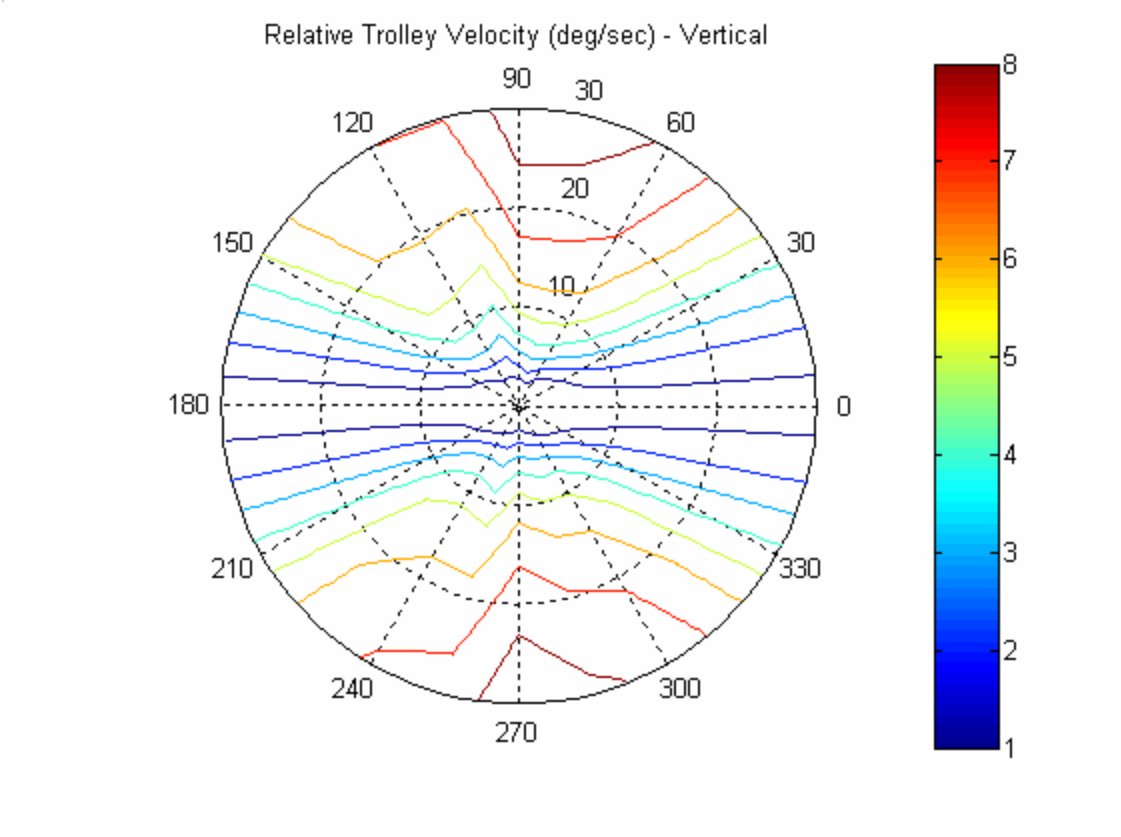

Figure 22. Relative Vertical Trolley Velocity (degrees/second)

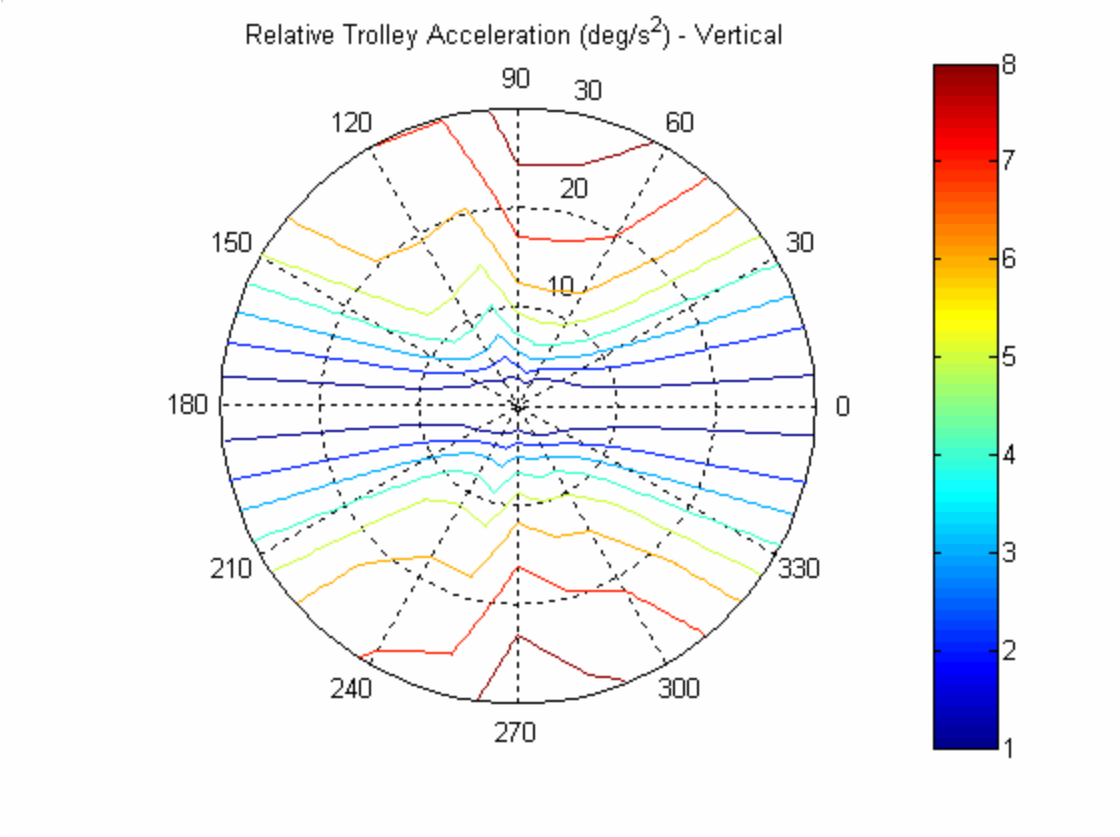

Figure 23. Relative Vertical Trolley Acceleration (degrees/second^2)

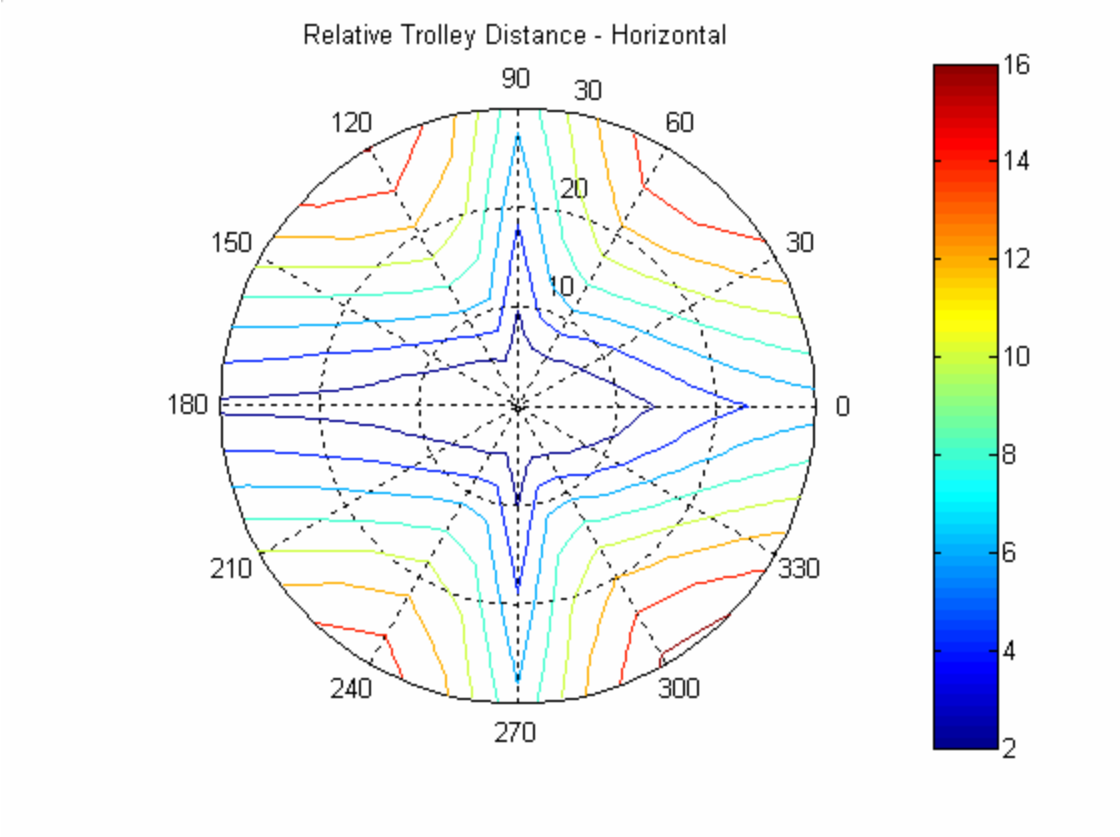

Figure 24. Relative Horizontal Trolley Distance (feet)

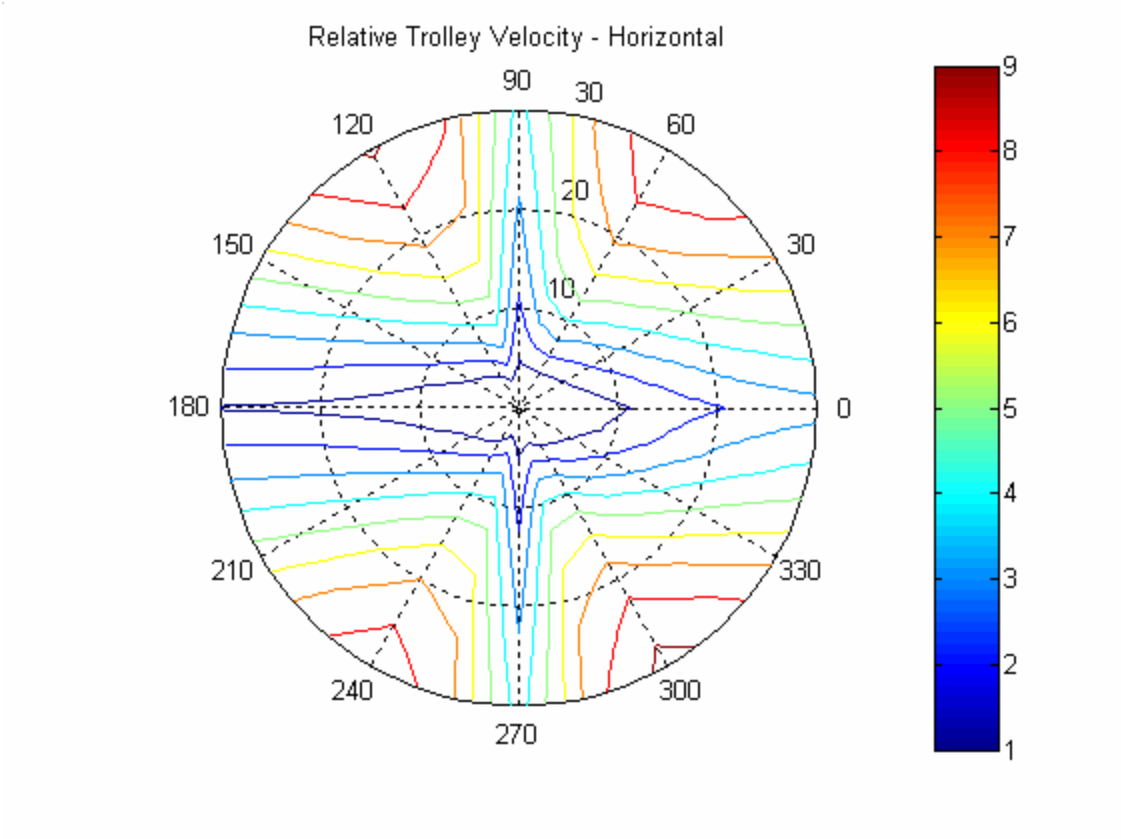

Figure 25. Relative Horizontal Trolley Velocity

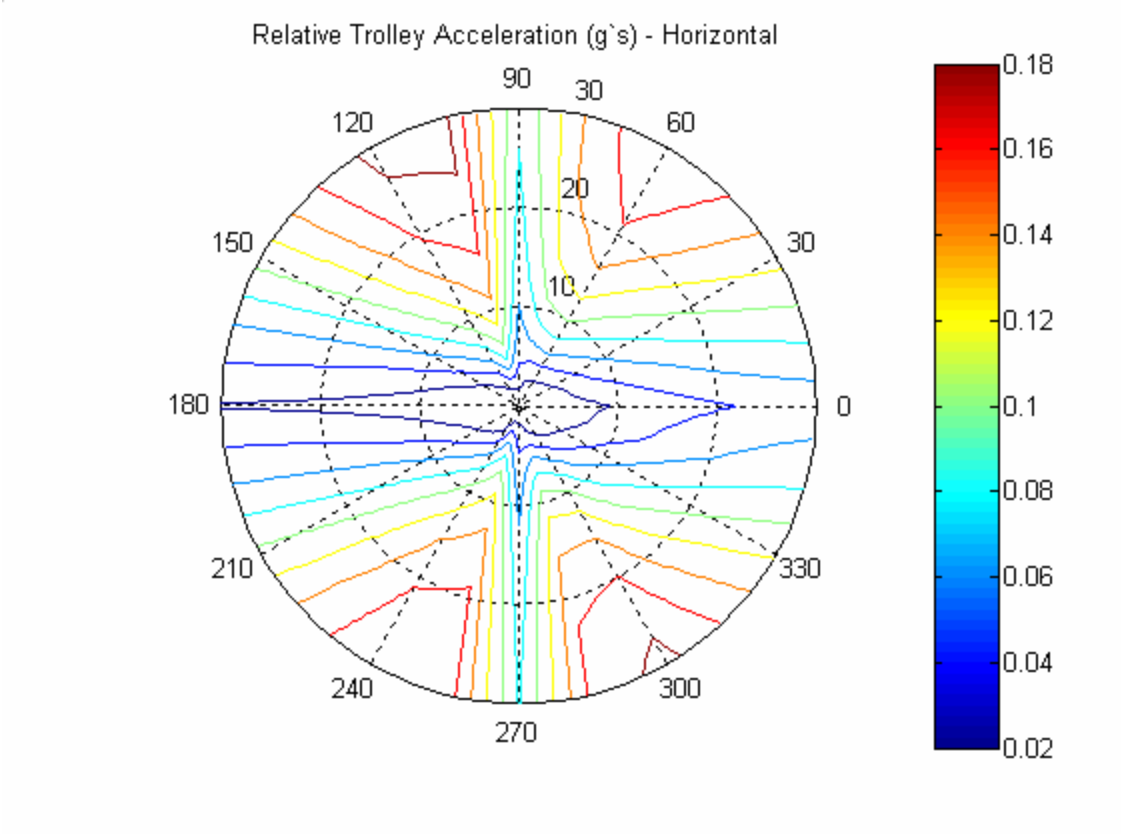

Figure 26. Relative Horizontal Trolley Acceleration

D. SUMMARY OF MODELING RESULTS

In terms of cargo transfer ability and throughput, one of the most important parameters is the angular deflection of the trolley mechanism between the two ends. This angle, which was presented in Figure (21), is reproduced here in a higher resolution form in Figure (27). It can be seen that the relative angular displacement is maximum for beam seas, and for sea state 5 and for the indicated conditions it is expected not to exceed 10 degrees RMS. The angle is considerably smaller for head and following seas. It should be emphasized that this angle is differential amplitude and it should be superimposed on the static equilibrium angle between the ship and the RRDF. For certain operations, where maximum cargo throughput is needed, this trolley relative angle can be used as the overarching optimization criterion in terms of vessels orientation with respect to the seaway. Maximum expected values for motions, velocities, and accelerations, both absolute and relative have been summarized in the previous sub-sections.

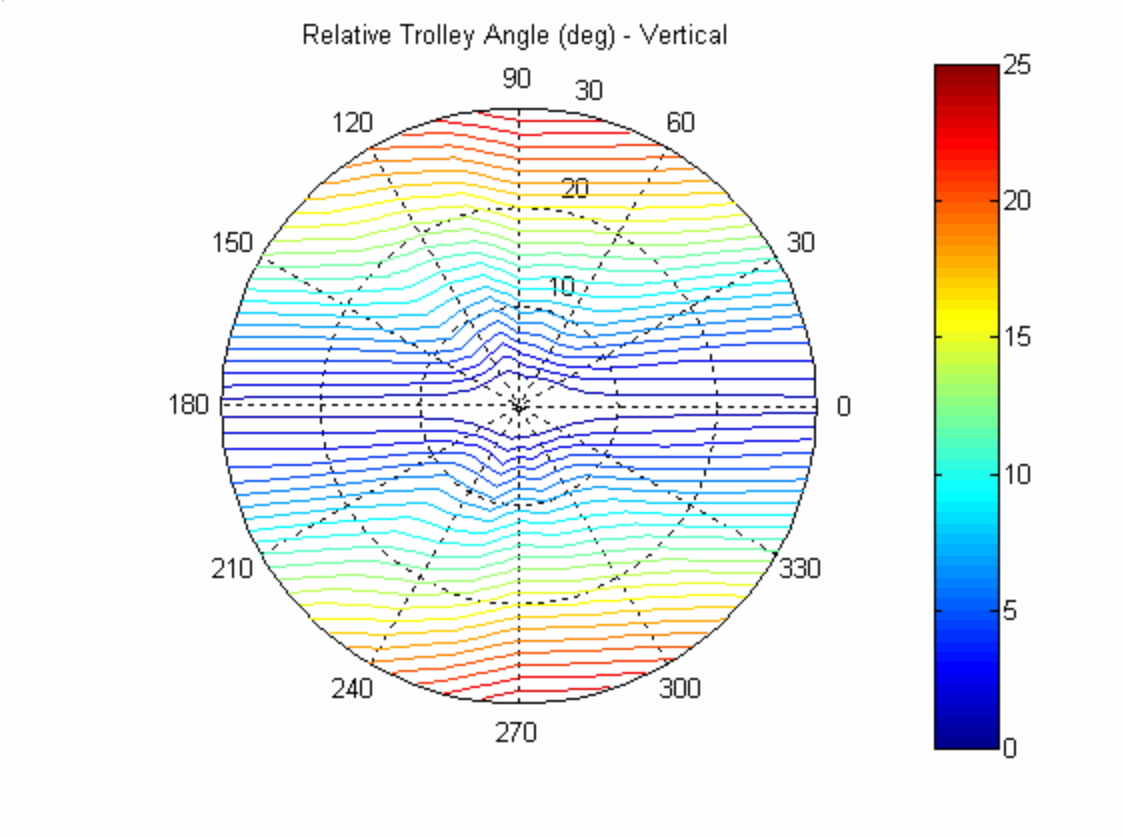

Figure 27. Relative Vertical Trolley Angle (degrees)

THIS PAGE INTENTIONALLY LEFT BLANK

V. TRANSFER RATE

It is difficult to compare the transfer rates of this trolley interface system with transfer rates of currently employed systems (such as ramps and cranes), because these two systems are employed differently. However, a basic comparison of transfer rates is done, in the case that these two systems were employed under similar conditions.

First, a standard number of vehicles and cargo is selected for transfer. The Marines at Naval Expeditionary Training Group Pacific (EWTGPAC, in San Diego) gave the current operational standard of time for the transfer of equipment and supplies associated with one Marine Expeditionary Brigade (MEB) ashore as 3-5 days. This is for sea state 1 conditions. Disregarding sea state, this indicates a transfer requirement that the performance of the trolley interface can be compared with. A MEB is not well defined, and so an approximation of gear required is used. References (1-3) define the major equipment of a MEB, and a summary of this data is provided in Tables (1-3).

Major Weapons	MEB	Weight per unit (ST)	Total Weight (ST)
LAV AT	4	14.20	56.80
LAV 25	14	14.20	198.80
LAV LOG	3	14.20	42.60
LAV RECOV	3	14.20	42.60
AAAVC7	9	35.45	319.05
AAAVR7	4	35.45	141.80
AAAVP7	96	35.45	3403.20
M1A1	58	67.70	3926.60
Armed HMMWV (TOW)	72	2.70	194.40
M198 How	30	7.88	236.40

Table 1. Major MEB Weapons

MT/Comm Equipment	MEB	Weight per unit (ST)	Total Weight (ST)
Armed HMMWV	57	3.00	171.00
LVS Power Unit	109	12.65	1378.85
LVS Wrecker	4	14.20	56.80
LVS Trailer	53	8.00	424.00
5 Ton	282	10.73	3025.86
P-19	8	16.80	134.40
HMMWV	473	2.60	1229.80
MRC-110	65	2.60	169.00
MRC-138	60	2.60	156.00
MRC-142	21	2.60	54.60
M970 Refueler	26	7.65	198.90

Table 2. MEB MT/Comm Equipment

Combat Eng./Eng. Support	MEB	Weight per unit (ST)	Total Weight (ST)
ROWPU	41	2.33	95.53
RTCH	14	58.48	818.72
D7	17	17.29	293.93
Extension Boom Forklift	46	13.00	598.00
TRAM	37	16.70	617.90
M9 ACE	6	18.00	108.00
MC1150 Tractor	7	13.90	97.30
Watercons	111	1.35	149.85

Table 3. MEB Combat Engineering/Engineering Support Equipment

Next, a method is created to estimate the transfer rate of the trolley. The system is modeled as a wheeled trolley, pulled along a 100 foot track. An electric motor pulls the trolley, with a cable that passes through one pulley. This setup is diagrammed in Figure (28).

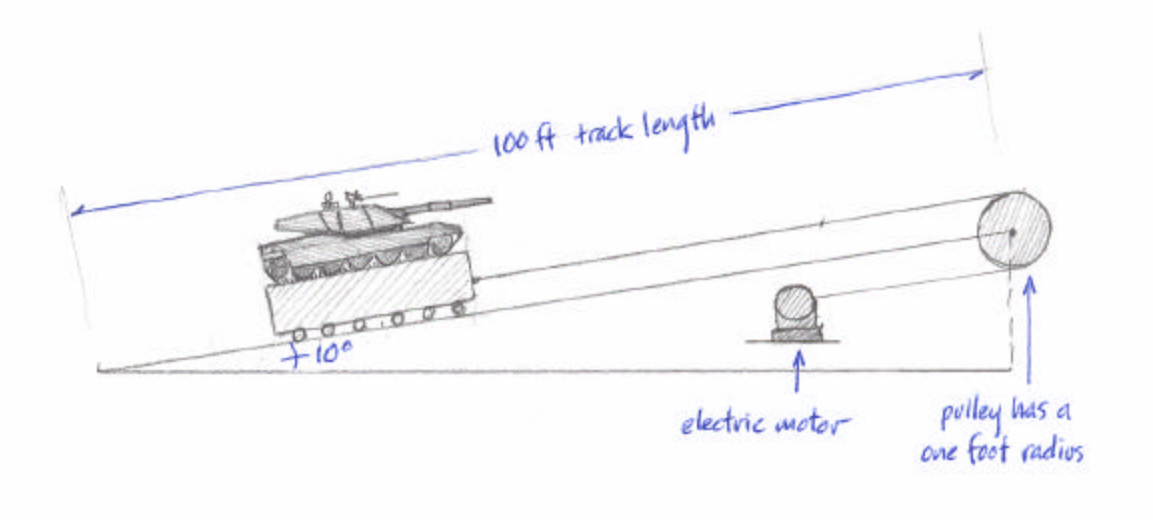

Figure 28. Diagram of Trolley System Model

Three power levels are selected for the motor: 100 hp, 300 hp and 500 hp. Other characteristics of the model are listed in Table (4):

Characteristic	Value	Units
Motor Power	100/300/500	Horsepower
Motor Efficiency	5	Percent
Wheel Bearing Losses	.05	μ
Weight of Trolley	12.5	Short Tons
Weight of Load	Vehicle Dependant	Short Tons
Diameter of Pulley	2	Feet
Angle of Inclination	10	Degrees
Gravity	32.2	Feet/sec^2

Table 4. Trolley Model Characteristics

Because the sea state that a transfer will be conducted in cannot be predicted, the worst case scenario is modeled. The data for relative motion between the TAKR ship and the RRDF indicates that the trolley will experience angles of up to 10 degrees in sea state 5. So the trolley is modeled as traveling up a track angled at 10 degrees.

The affects of accelerations and velocities on the movement of the trolley along the track are not accounted for. That level of analysis was determined to be excessive for the rough order of the undertaken estimation.

Time for a trolley transfer is based on the velocity of the trolley:

$$Time = \frac{V}{x} \tag{14}$$

where V = trolley velocity and x = track length.

Velocity can be determined by the rotational speed of the pulley, using the relation:

$$V = rw \tag{15}$$

where ? = rotational velocity of the pulley and r = radius of the pulley.

Power can be defined with the following equation:

$$Power = \frac{M * n}{E_m} \tag{16}$$

where M=moment, n=rotational speed (radians/sec) and E_m=Motor Efficiency.

With a cable traveling over a pully, the moment is defined by:

$$M = F * r \tag{17}$$

where F=force and r=radius of the pulley

In this case, with the cable pulling the trolley up a 10 degree incline, the force exerted on the cable is:

$$F = mg\sin(q) + mmg\cos(q) \tag{18}$$

where m = combined mass of the trolley and load, g = gravity, ? = angle of inclination (10 degrees) and μ = coefficient of friction (for the 24 wheels of the cart). Putting these equations together, one equation is found that determines the time for one trolley trip, based on the values listed in Table (4):

$$TransferTime = \frac{Power * E_m}{\left[mg\sin(q) + mmg\cos(q)\right] * r^2 * 100} \tag{19}$$

and we know that maximum velocity is defined as:

$$V_{\max} = \frac{Power * E_m}{mg(\sin(q) + m\cos(q))} \tag{20}$$

So transfer time becomes:

$$TransferTime = \frac{V}{r^2 * 100} \tag{21}$$

To account for acceleration and deceleration of the trolley at each end of the rails, a transfer speed V of ¼ the maximum velocity is used. The transfer of one vehicle involves the following steps: A vehicle is loaded onto the trolley, transferred across the rails, the vehicle is unloaded from the trolley, and then the empty trolley is brought back across the rails. Loading and unloading times are assumed to be 4 minutes each. Using this information, and the above relations, a spreadsheet was created in Microsoft Excel to determine the required time to transfer each of the vehicles listed in Tables (1-3). Table (5) lists the resulting transfer times.

	100 HP motor	300 HP motor	500 HP motor
Time to transfer 1 MEB, using 1 trolley system (days)	12.92	11.61	11.35
Time to transfer 1 MEB, using 4 trolley systems (days)	3.23	2.90	2.84

Table 5. Calculated Transfer Speeds

Total transfer time when using only one trolley system is high, around 12 days in each case. However, MEBs are usually contained on at least 4 MPF ships, and so at least 4 of these systems would be operating, reducing the transfer time to around 3 days. This rate is similar to current transfer times, as given by EWTGPAC.

There are many other factors that affect transfer rates. When conducting offloading operations further off the coast, as the Marine Corps is planning to do, transit from ship to shore becomes very time consuming, and will have to be taken into account. Implementing STOM means only sending equipment ashore that is needed. This keeps the operational footprint light, and could greatly reduce at sea transfer requirements. A

reliability factor will also have to be designed into the offload model as well, because nothing has 100% operational reliability.

A more in-depth analysis of this model would also take acceleration of the cart into account, when determining the transit time of the trolley down the length of the rails. To do this, a differential equation must be solved:

$$P = \left[m\frac{d^2x}{dt^2} + mmg\cos(q) + mg\sin(q) \right] * \left(\frac{dx}{dt} \right) \tag{22}$$

where x = distance along the track and m = mass of the loaded trolley. Even more difficult would be to analyze the affects of the accelerations and decelerations of the entire structure on the trolley, as it is moving relative to the two ships, changing the weight of the trolley as it moves along the tracks.

VI. CONCLUSIONS AND RECOMMENDATIONS

A. CONCLUSIONS

This thesis has laid the foundation for follow up studies on a new trolley-like interface for ship-to-ship cargo transfer. The proposed technique can be used for both military operations (such as expeditionary warfare) but also in commercial applications. The response of the system has been analyzed in terms of its expected values in a seaway. Basic response characteristics include ship and trolley motions, velocities, and accelerations both absolute and relative. A preliminary assessment of the expected transfer rates shows that the system should be sufficient in order to meet Marine Corps needs in amphibious warfare. It is expected that the proposed system will offer enhanced cargo throughput and operational availability over existing systems. In order to fully justify the potential capabilities of the proposed system, the following items must be completed:

B. RECOMMENDATION FOR FUTURE WORK

1. Short Crested Seas

Adding another degree of realism into seaway modeling can be done by introducing a directionality spreading function. Such seas are called short-crested and can model actual seas better, since a unique sea directional angle does not exist. Instead, the energy of the seaway is assumed to spread over a range of directions. The directional spreading model that will be employed in this phase is:

$$S(w,q) = S(w)\Theta(q) \tag{23}$$

where

$$\Theta(q) = \frac{2}{p}\cos^2 q \tag{24}$$

and $S(w)$ is the two-parameter Bretschneider spectrum.

2. Side Trolley Placement

The case of a side trolley placement is particularly interesting, especially for the ship-to-RRDF cargo transfer case. The reason for this is that there is considerable hydrodynamic interaction from the ship to the RRDF. Beam seas can result in the RRDF being either sheltered by the presence of the body, or exposed to both the incoming wave system and the wave system that is diffracted by the presence of the body. Depending on phase angle difference, the resulting wave excitation can be significantly magnified compared to the open water case. Further analysis of this can determine if side placement of the trolley interface is feasible.

3. Structural Coupling

Finally, we need to evaluate the structural response of the trolley mechanism for a given end-point excitation in terms of prescribed motions. Torsion and bending are particularly important, especially for a heavily loaded trolley. Depending on the boundary conditions, it may be necessary to iterate between the hydrodynamic and the structural analysis programs to assess the influence of the trolley on RRDF motions. The influence of trolley response on the ship is small and can be neglected.

APPENDIX A

ACRONYMS

AAAV	Advanced Amphibious Attach Vehicle
ADC	Advanced Design Consulting, Inc.
EWTGPAC	Expeditionary Warfare Training Group Pacific
GCE	Ground Combat Element
HMMWV	High Mobility Multipurpose Wheeled Vehicle
LAV	Light Armored Vehicle
LHA	Amphibious Assault Ship, General Purpose
LHD	Amphibious Assault Ship, Multi Purpose
LMSR	Large Medium Speed Roll-on/Roll-off Ship
LVS	Logistics Vehicle System
MEB	Marine Expeditionary Brigade
MPF	Maritime Prepositioned Force
MSC	Military Sealift Command
RMS	Root Mean Squared
RO/RO	Roll-On/Roll-Off
RRDF	Roll-on Roll-off Discharge Facility
ST	Short Ton
STOM	Ship to Objective Maneuver
TOW	Tube Launched, Optically Tracked, Wire-Guided [Missile]
TAKR	MSC controlled Ro-Ro Ship crewed with civilians
WAMIT	Wave Analysis, Massachusetts Institute of Technology

THIS PAGE INTENTIONALLY LEFT BLANK

APPENDIX B

MATLAB CODE

```
% Motions calculation for CapeD/RRDF/trolley interface.
% Long-crested Bretchneider seas.
%
i_seaway=input('Enter 0 for PM or 1 for Bretchneider spectrum = ');
if i_seaway == 1
   T_m =input('Modal Period (sec) = ');
   omega_m=2*pi/T_m;
end
%
x_arm_CAPED_1=-330;
x_arm_CAPED_2=-330;
y_arm_CAPED_1=-10;
y_arm_CAPED_2=+10;
x_arm_RRDF_1=20;
x_arm_RRDF_2=20;
y_arm_RRDF_1=-10;
y_arm_RRDF_2=+10;
trolley_length=100;
%
% Load processed WAMIT data file
%
load CAPED
NH=25;
i_NH=15;
%
% Set the frequencies vector (0.3 to 2.5 rad/sec)
%
NF=(size(frequencies));
NF=NF(1,1);
w=frequencies;
%
% Set the headings vector (0 to 360 degrees in i_NH deg. increments)
%
for i=1:NH,
   heading(i)=i_NH*(i-1);
end
%
% Set added mass and damping matrices and forcing vector
%
for i=1:NF,
   i_string=num2str(i);
```

```
    A(:,:,i)=eval(strcat('admassfreq',i_string));
    B(:,:,i)=eval(strcat('addumpingfreq',i_string));
    for j=1:NH,
        j_string=num2str(j);
        if j==NH
            j_string=num2str(1);
        end
        F(:,i,j)=eval(strcat('forcfreq',i_string,'head',j_string));
    end
end
%
% Loop on sea direction
%
ibeta=0;
beta_incr=i_NH;
imag_unit=sqrt(-1);
for beta=0:beta_incr:360,
    ibeta=ibeta+1;
    heading_single=heading(ibeta);
    %
    % Frequency domain response is given by x= [-w^2*(A+mass)+i*w*B+C]^(-1)*F
    %
    for i=1:NF,
        w_single=w(i);
        A_bar=-w_single*w_single*(A(:,:,i))+imag_unit*w_single*B(:,:,i)+C;
        F_bar=F(:,i,ibeta);
        x=inv(A_bar)*F_bar;
        %
        % Ship motions
        %
        surge_CAPED(i) = x(1);
        heave_CAPED(i) = x(2);
        sway_CAPED(i)  = x(3);
        roll_CAPED(i)  = x(4);
        pitch_CAPED(i) = x(5);
        yaw_CAPED(i)   = x(6);
        %
        % RRDF motions
        %
        surge_RRDF(i) = x(7);
        heave_RRDF(i) = x(8);
        sway_RRDF(i)  = x(9);
        roll_RRDF(i)  = x(10);
        pitch_RRDF(i) = x(11);
        yaw_RRDF(i)   = x(12);
        %
```

```
% Motions/velocities/accelerations at trolley end - CAPED side
%
m_t_CAPED_v_1(i)=heave_CAPED(i)-x_arm_CAPED_1*pitch_CAPED(i)...
   -y_arm_CAPED_1*roll_CAPED(i);
m_t_CAPED_v_2(i)=heave_CAPED(i)-x_arm_CAPED_2*pitch_CAPED(i)...
   -y_arm_CAPED_2*roll_CAPED(i);
m_t_CAPED_h_1(i)=sway_CAPED(i)+x_arm_CAPED_1*yaw_CAPED(i));
m_t_CAPED_h_2(i)=sway_CAPED(i)+x_arm_CAPED_2*yaw_CAPED(i);
v_t_CAPED_v_1(i)=imag_unit*w_single*m_t_CAPED_v_1(i);
v_t_CAPED_v_2(i)=imag_unit*w_single*m_t_CAPED_v_2(i);
v_t_CAPED_h_1(i)=imag_unit*w_single*m_t_CAPED_h_1(i);
v_t_CAPED_h_2(i)=imag_unit*w_single*m_t_CAPED_h_2(i);
a_t_CAPED_v_1(i)=-w_single*w_single*m_t_CAPED_v_1(i);
a_t_CAPED_v_2(i)=-w_single*w_single*m_t_CAPED_v_2(i);
a_t_CAPED_h_1(i)=-w_single*w_single*m_t_CAPED_h_1(i);
a_t_CAPED_h_2(i)=-w_single*w_single*m_t_CAPED_h_2(i);
%
% Motions/velocities/accelerations at trolley end - RRDF side
%
m_t_RRDF_v_1(i)=heave_RRDF(i)-x_arm_RRDF_1*pitch_RRDF(i);
m_t_RRDF_v_2(i)=heave_RRDF(i)-x_arm_RRDF_2*pitch_RRDF(i);
m_t_RRDF_h_1(i)=sway_RRDF(i)+x_arm_RRDF_1*yaw_RRDF(i);
m_t_RRDF_h_2(i)=sway_RRDF(i)+x_arm_RRDF_2*yaw_RRDF(i);
v_t_RRDF_v_1(i)=imag_unit*w_single*m_t_RRDF_v_1(i);
v_t_RRDF_v_2(i)=imag_unit*w_single*m_t_RRDF_v_2(i);
v_t_RRDF_h_1(i)=imag_unit*w_single*m_t_RRDF_h_1(i);
v_t_RRDF_h_2(i)=imag_unit*w_single*m_t_RRDF_h_2(i);
a_t_RRDF_v_1(i)=-w_single*w_single*m_t_RRDF_v_1(i);
a_t_RRDF_v_2(i)=-w_single*w_single*m_t_RRDF_v_2(i);
a_t_RRDF_h_1(i)=-w_single*w_single*m_t_RRDF_h_1(i);
a_t_RRDF_h_2(i)=-w_single*w_single*m_t_RRDF_h_2(i);
%
% Trolley relative vertical angular displacement
%
m_trolley_angle_v_1(i)=(m_t_CAPED_v_1(i)-m_t_RRDF_v_1(i))/trolley_length;
m_trolley_angle_v_2(i)=(m_t_CAPED_v_2(i)-m_t_RRDF_v_2(i))/trolley_length;
v_trolley_angle_v_1(i)=imag_unit*w_single*m_trolley_angle_v_1(i);
v_trolley_angle_v_2(i)=imag_unit*w_single*m_trolley_angle_v_2(i);
a_trolley_angle_v_1(i)=-w_single*w_single*m_trolley_angle_v_1(i);
a_trolley_angle_v_2(i)=-w_single*w_single*m_trolley_angle_v_2(i);
m_trolley_angle_v_twist(i)=m_trolley_angle_v_1(i)-m_trolley_angle_v_2(i);

m_trolley_angle_v_average(i)=0.5*(m_trolley_angle_v_1(i)+m_trolley_angle_v_2(i));
%
% Trolley relative horizontal displacement
%
```

```
    m_trolley_distance_h_1(i)=(m_t_CAPED_h_1(i)-m_t_RRDF_h_1(i));
    m_trolley_distance_h_2(i)=(m_t_CAPED_h_2(i)-m_t_RRDF_h_2(i));
    v_trolley_distance_h_1(i)=imag_unit*w_single*m_trolley_distance_h_1(i);
    v_trolley_distance_h_2(i)=imag_unit*w_single*m_trolley_distance_h_2(i);
    a_trolley_distance_h_1(i)=-w_single*w_single*m_trolley_distance_h_1(i);
    a_trolley_distance_h_2(i)=-w_single*w_single*m_trolley_distance_h_2(i);
end
%
% Random wave calculations
% Bretchneider spectrum
%
iHS=0;
for HS=0.5:0.5:30,              % Loop on significant wave height
    iHS=iHS+1;
    if i_seaway ==0
       omega_m=0.4*sqrt(32.2/HS);
    end
    A_s=(1.25/4)*(omega_m^4)*(HS^2);
    B_s=1.25*omega_m^4;
    S=(A_s./w.^5).*exp(-B_s./w.^4);
    %
    % Define response spectra
    %
    S_surge_CAPED = ((abs(surge_CAPED)).^2).*S';
    S_surge_RRDF  = ((abs(surge_RRDF)).^2).*S';
    S_heave_CAPED = ((abs(heave_CAPED)).^2).*S';
    S_heave_RRDF  = ((abs(heave_RRDF)).^2).*S';
    S_sway_CAPED  = ((abs(sway_CAPED)).^2).*S';
    S_sway_RRDF   = ((abs(sway_RRDF)).^2).*S';
    S_roll_CAPED  = ((abs(roll_CAPED)).^2).*S';
    S_roll_RRDF   = ((abs(roll_RRDF)).^2).*S';
    S_pitch_CAPED = ((abs(pitch_CAPED)).^2).*S';
    S_pitch_RRDF  = ((abs(pitch_RRDF)).^2).*S';
    S_yaw_CAPED   = ((abs(yaw_CAPED)).^2).*S';
    S_yaw_RRDF    = ((abs(yaw_RRDF)).^2).*S';
    S_m_t_CAPED_v_1 = ((abs(m_t_CAPED_v_1)).^2).*S';
    S_m_t_CAPED_v_2 = ((abs(m_t_CAPED_v_2)).^2).*S';
    S_m_t_CAPED_h_1 = ((abs(m_t_CAPED_h_1)).^2).*S';
    S_m_t_CAPED_h_2 = ((abs(m_t_CAPED_h_2)).^2).*S';
    S_v_t_CAPED_v_1 = ((abs(v_t_CAPED_v_1)).^2).*S';
    S_v_t_CAPED_v_2 = ((abs(v_t_CAPED_v_2)).^2).*S';
    S_v_t_CAPED_h_1 = ((abs(v_t_CAPED_h_1)).^2).*S';
    S_v_t_CAPED_h_2 = ((abs(v_t_CAPED_h_2)).^2).*S';
    S_a_t_CAPED_v_1 = ((abs(a_t_CAPED_v_1)).^2).*S';
    S_a_t_CAPED_v_2 = ((abs(a_t_CAPED_v_2)).^2).*S';
    S_a_t_CAPED_h_1 = ((abs(a_t_CAPED_h_1)).^2).*S';
```

```
S_a_t_CAPED_h_2 = ((abs(a_t_CAPED_h_2)).^2).*S';
S_m_t_RRDF_v_1  = ((abs(m_t_RRDF_v_1)).^2).*S';
S_m_t_RRDF_v_2  = ((abs(m_t_RRDF_v_2)).^2).*S';
S_m_t_RRDF_h_1  = ((abs(m_t_RRDF_h_1)).^2).*S';
S_m_t_RRDF_h_2  = ((abs(m_t_RRDF_h_2)).^2).*S';
S_v_t_RRDF_v_1  = ((abs(v_t_RRDF_v_1)).^2).*S';
S_v_t_RRDF_v_2  = ((abs(v_t_RRDF_v_2)).^2).*S';
S_v_t_RRDF_h_1  = ((abs(v_t_RRDF_h_1)).^2).*S';
S_v_t_RRDF_h_2  = ((abs(v_t_RRDF_h_2)).^2).*S';
S_a_t_RRDF_v_1  = ((abs(a_t_RRDF_v_1)).^2).*S';
S_a_t_RRDF_v_2  = ((abs(a_t_RRDF_v_2)).^2).*S';
S_a_t_RRDF_h_1  = ((abs(a_t_RRDF_h_1)).^2).*S';
S_a_t_RRDF_h_2  = ((abs(a_t_RRDF_h_2)).^2).*S';
S_m_trolley_angle_v_1 = ((abs(m_trolley_angle_v_1)).^2).*S';
S_m_trolley_angle_v_2 = ((abs(m_trolley_angle_v_2)).^2).*S';
S_v_trolley_angle_v_1 = ((abs(v_trolley_angle_v_1)).^2).*S';
S_v_trolley_angle_v_2 = ((abs(v_trolley_angle_v_2)).^2).*S';
S_a_trolley_angle_v_1 = ((abs(a_trolley_angle_v_1)).^2).*S';
S_a_trolley_angle_v_2 = ((abs(a_trolley_angle_v_2)).^2).*S';
S_m_trolley_angle_v_twist = ((abs(m_trolley_angle_v_twist)).^2).*S';
S_m_trolley_angle_v_average = ((abs(m_trolley_angle_v_average)).^2).*S';
S_m_trolley_distance_h_1 = ((abs(m_trolley_distance_h_1)).^2).*S';
S_m_trolley_distance_h_2 = ((abs(m_trolley_distance_h_2)).^2).*S';
S_v_trolley_distance_h_1 = ((abs(v_trolley_distance_h_1)).^2).*S';
S_v_trolley_distance_h_2 = ((abs(v_trolley_distance_h_2)).^2).*S';
S_a_trolley_distance_h_1 = ((abs(a_trolley_distance_h_1)).^2).*S';
S_a_trolley_distance_h_2 = ((abs(a_trolley_distance_h_2)).^2).*S';
%
% Integral initializations
%
S_surge_CAPED_i = 0;
S_surge_RRDF_i  = 0;
S_heave_CAPED_i = 0;
S_heave_RRDF_i  = 0;
S_sway_CAPED_i  = 0;
S_sway_RRDF_i   = 0;
S_roll_CAPED_i  = 0;
S_roll_RRDF_i   = 0;
S_pitch_CAPED_i = 0;
S_pitch_RRDF_i  = 0;
S_yaw_CAPED_i   = 0;
S_yaw_RRDF_i    = 0;
S_m_t_CAPED_v_1_i = 0;
S_m_t_CAPED_h_1_i = 0;
S_v_t_CAPED_v_1_i = 0;
S_v_t_CAPED_h_1_i = 0;
```

```
S_a_t_CAPED_v_1_i = 0;
S_a_t_CAPED_h_1_i = 0;
S_m_t_RRDF_v_1_i  = 0;
S_m_t_RRDF_h_1_i  = 0;
S_v_t_RRDF_v_1_i  = 0;
S_v_t_RRDF_h_1_i  = 0;
S_a_t_RRDF_v_1_i  = 0;
S_a_t_RRDF_h_1_i  = 0;
S_m_trolley_angle_v_1_i = 0;
S_v_trolley_angle_v_1_i = 0;
S_a_trolley_angle_v_1_i = 0;
S_m_trolley_distance_h_1_i = 0;
S_v_trolley_distance_h_1_i = 0;
S_a_trolley_distance_h_1_i = 0;
S_m_t_CAPED_v_2_i = 0;
S_m_t_CAPED_h_2_i = 0;
S_v_t_CAPED_v_2_i = 0;
S_v_t_CAPED_h_2_i = 0;
S_a_t_CAPED_v_2_i = 0;
S_a_t_CAPED_h_2_i = 0;
S_m_t_RRDF_v_2_i  = 0;
S_m_t_RRDF_h_2_i  = 0;
S_v_t_RRDF_v_2_i  = 0;
S_v_t_RRDF_h_2_i  = 0;
S_a_t_RRDF_v_2_i  = 0;
S_a_t_RRDF_h_2_i  = 0;
S_m_trolley_angle_v_2_i = 0;
S_v_trolley_angle_v_2_i = 0;
S_a_trolley_angle_v_2_i = 0;
S_m_trolley_distance_h_2_i = 0;
S_v_trolley_distance_h_2_i = 0;
S_a_trolley_distance_h_2_i = 0;
S_m_trolley_angle_v_twist_i = 0;
S_m_trolley_angle_v_average_i = 0;
%
% Integral S(w)*|RAO(w)|^2
%
for i=2:1:NF,
   avg_value=0.5*(S_surge_CAPED(i)+S_surge_CAPED(i-1));
   S_surge_CAPED_i = S_surge_CAPED_i+avg_value*abs(w(i-1)-w(i));
   avg_value=0.5*(S_surge_RRDF(i)+S_surge_RRDF(i-1));
   S_surge_RRDF_i  = S_surge_RRDF_i+avg_value*abs(w(i-1)-w(i));
   avg_value=0.5*(S_heave_CAPED(i)+S_heave_CAPED(i-1));
   S_heave_CAPED_i = S_heave_CAPED_i+avg_value*abs(w(i-1)-w(i));
   avg_value=0.5*(S_heave_RRDF(i)+S_heave_RRDF(i-1));
   S_heave_RRDF_i  = S_heave_RRDF_i+avg_value*abs(w(i-1)-w(i));
```

```
avg_value=0.5*(S_sway_CAPED(i)+S_sway_CAPED(i-1));
S_sway_CAPED_i  = S_sway_CAPED_i+avg_value*abs(w(i-1)-w(i));
avg_value=0.5*(S_sway_RRDF(i)+S_sway_RRDF(i-1));
S_sway_RRDF_i   = S_sway_RRDF_i+avg_value*abs(w(i-1)-w(i));
avg_value=0.5*(S_roll_CAPED(i)+S_roll_CAPED(i-1));
S_roll_CAPED_i  = S_roll_CAPED_i+avg_value*abs(w(i-1)-w(i));
avg_value=0.5*(S_roll_RRDF(i)+S_roll_RRDF(i-1));
S_roll_RRDF_i   = S_roll_RRDF_i+avg_value*abs(w(i-1)-w(i));
avg_value=0.5*(S_pitch_CAPED(i)+S_pitch_CAPED(i-1));
S_pitch_CAPED_i = S_pitch_CAPED_i+avg_value*abs(w(i-1)-w(i));
avg_value=0.5*(S_pitch_RRDF(i)+S_pitch_RRDF(i-1));
S_pitch_RRDF_i  = S_pitch_RRDF_i+avg_value*abs(w(i-1)-w(i));
avg_value=0.5*(S_yaw_CAPED(i)+S_yaw_CAPED(i-1));
S_yaw_CAPED_i   = S_yaw_CAPED_i+avg_value*abs(w(i-1)-w(i));
avg_value=0.5*(S_yaw_RRDF(i)+S_yaw_RRDF(i-1));
S_yaw_RRDF_i    = S_yaw_RRDF_i+avg_value*abs(w(i-1)-w(i));
%
% Calculations for point "1"
%
avg_value=0.5*(S_m_t_CAPED_v_1(i)+S_m_t_CAPED_v_1(i-1));
S_m_t_CAPED_v_1_i = S_m_t_CAPED_v_1_i+avg_value*abs(w(i-1)-w(i));
avg_value=0.5*(S_m_t_CAPED_h_1(i)+S_m_t_CAPED_h_1(i-1));
S_m_t_CAPED_h_1_i = S_m_t_CAPED_h_1_i+avg_value*abs(w(i-1)-w(i));
avg_value=0.5*(S_v_t_CAPED_v_1(i)+S_v_t_CAPED_v_1(i-1));
S_v_t_CAPED_v_1_i = S_v_t_CAPED_v_1_i+avg_value*abs(w(i-1)-w(i));
avg_value=0.5*(S_v_t_CAPED_h_1(i)+S_v_t_CAPED_h_1(i-1));
S_v_t_CAPED_h_1_i = S_v_t_CAPED_h_1_i+avg_value*abs(w(i-1)-w(i));
avg_value=0.5*(S_a_t_CAPED_v_1(i)+S_a_t_CAPED_v_1(i-1));
S_a_t_CAPED_v_1_i = S_a_t_CAPED_v_1_i+avg_value*abs(w(i-1)-w(i));
avg_value=0.5*(S_a_t_CAPED_h_1(i)+S_a_t_CAPED_h_1(i-1));
S_a_t_CAPED_h_1_i = S_a_t_CAPED_h_1_i+avg_value*abs(w(i-1)-w(i));
avg_value=0.5*(S_m_t_RRDF_v_1(i)+S_m_t_RRDF_v_1(i-1));
S_m_t_RRDF_v_1_i  = S_m_t_RRDF_v_1_i+avg_value*abs(w(i-1)-w(i));
avg_value=0.5*(S_m_t_RRDF_h_1(i)+S_m_t_RRDF_h_1(i-1));
S_m_t_RRDF_h_1_i  = S_m_t_RRDF_h_1_i+avg_value*abs(w(i-1)-w(i));
avg_value=0.5*(S_v_t_RRDF_v_1(i)+S_v_t_RRDF_v_1(i-1));
S_v_t_RRDF_v_1_i  = S_v_t_RRDF_v_1_i+avg_value*abs(w(i-1)-w(i));
avg_value=0.5*(S_v_t_RRDF_h_1(i)+S_v_t_RRDF_h_1(i-1));
S_v_t_RRDF_h_1_i  = S_v_t_RRDF_h_1_i+avg_value*abs(w(i-1)-w(i));
avg_value=0.5*(S_a_t_RRDF_v_1(i)+S_a_t_RRDF_v_1(i-1));
S_a_t_RRDF_v_1_i  = S_a_t_RRDF_v_1_i+avg_value*abs(w(i-1)-w(i));
avg_value=0.5*(S_a_t_RRDF_h_1(i)+S_a_t_RRDF_h_1(i-1));
S_a_t_RRDF_h_1_i  = S_a_t_RRDF_h_1_i+avg_value*abs(w(i-1)-w(i));
avg_value=0.5*(S_m_trolley_angle_v_1(i)+S_m_trolley_angle_v_1(i-1));
S_m_trolley_angle_v_1_i = S_m_trolley_angle_v_1_i+...
   avg_value*abs(w(i-1)-w(i));
```

```
avg_value=0.5*(S_v_trolley_angle_v_1(i)+S_v_trolley_angle_v_1(i-1));
S_v_trolley_angle_v_1_i = S_v_trolley_angle_v_1_i+...
   avg_value*abs(w(i-1)-w(i));
avg_value=0.5*(S_a_trolley_angle_v_1(i)+S_a_trolley_angle_v_1(i-1));
S_a_trolley_angle_v_1_i = S_a_trolley_angle_v_1_i+...
   avg_value*abs(w(i-1)-w(i));
avg_value=0.5*(S_m_trolley_distance_h_1(i)+S_m_trolley_distance_h_1(i-1));
S_m_trolley_distance_h_1_i = S_m_trolley_distance_h_1_i+...
   avg_value*abs(w(i-1)-w(i));
avg_value=0.5*(S_v_trolley_distance_h_1(i)+S_v_trolley_distance_h_1(i-1));
S_v_trolley_distance_h_1_i = S_v_trolley_distance_h_1_i+...
   avg_value*abs(w(i-1)-w(i));
avg_value=0.5*(S_a_trolley_distance_h_1(i)+S_a_trolley_distance_h_1(i-1));
S_a_trolley_distance_h_1_i = S_a_trolley_distance_h_1_i+...
   avg_value*abs(w(i-1)-w(i));
%
% Calculations for point "2 "
%
avg_value=0.5*(S_m_t_CAPED_v_2(i)+S_m_t_CAPED_v_2(i-1));
S_m_t_CAPED_v_2_i = S_m_t_CAPED_v_2_i+avg_value*abs(w(i-1)-w(i));
avg_value=0.5*(S_m_t_CAPED_h_2(i)+S_m_t_CAPED_h_2(i-1));
S_m_t_CAPED_h_2_i = S_m_t_CAPED_h_2_i+avg_value*abs(w(i-1)-w(i));
avg_value=0.5*(S_v_t_CAPED_v_2(i)+S_v_t_CAPED_v_2(i-1));
S_v_t_CAPED_v_2_i = S_v_t_CAPED_v_2_i+avg_value*abs(w(i-1)-w(i));
avg_value=0.5*(S_v_t_CAPED_h_2(i)+S_v_t_CAPED_h_2(i-1));
S_v_t_CAPED_h_2_i = S_v_t_CAPED_h_2_i+avg_value*abs(w(i-1)-w(i));
avg_value=0.5*(S_a_t_CAPED_v_2(i)+S_a_t_CAPED_v_2(i-1));
S_a_t_CAPED_v_2_i = S_a_t_CAPED_v_2_i+avg_value*abs(w(i-1)-w(i));
avg_value=0.5*(S_a_t_CAPED_h_2(i)+S_a_t_CAPED_h_2(i-1));
S_a_t_CAPED_h_2_i = S_a_t_CAPED_h_2_i+avg_value*abs(w(i-1)-w(i));
avg_value=0.5*(S_m_t_RRDF_v_2(i)+S_m_t_RRDF_v_2(i-1));
S_m_t_RRDF_v_2_i  = S_m_t_RRDF_v_2_i+avg_value*abs(w(i-1)-w(i));
avg_value=0.5*(S_m_t_RRDF_h_2(i)+S_m_t_RRDF_h_2(i-1));
S_m_t_RRDF_h_2_i  = S_m_t_RRDF_h_2_i+avg_value*abs(w(i-1)-w(i));
avg_value=0.5*(S_v_t_RRDF_v_2(i)+S_v_t_RRDF_v_2(i-1));
S_v_t_RRDF_v_2_i  = S_v_t_RRDF_v_2_i+avg_value*abs(w(i-1)-w(i));
avg_value=0.5*(S_v_t_RRDF_h_2(i)+S_v_t_RRDF_h_2(i-1));
S_v_t_RRDF_h_2_i  = S_v_t_RRDF_h_2_i+avg_value*abs(w(i-1)-w(i));
avg_value=0.5*(S_a_t_RRDF_v_2(i)+S_a_t_RRDF_v_2(i-1));
S_a_t_RRDF_v_2_i  = S_a_t_RRDF_v_2_i+avg_value*abs(w(i-1)-w(i));
avg_value=0.5*(S_a_t_RRDF_h_2(i)+S_a_t_RRDF_h_2(i-1));
S_a_t_RRDF_h_2_i  = S_a_t_RRDF_h_2_i+avg_value*abs(w(i-1)-w(i));
avg_value=0.5*(S_m_trolley_angle_v_2(i)+S_m_trolley_angle_v_2(i-1));
S_m_trolley_angle_v_2_i = S_m_trolley_angle_v_2_i+...
   avg_value*abs(w(i-1)-w(i));
avg_value=0.5*(S_v_trolley_angle_v_2(i)+S_v_trolley_angle_v_2(i-1));
```

```
        S_v_trolley_angle_v_2_i = S_v_trolley_angle_v_2_i+...
           avg_value*abs(w(i-1)-w(i));
        avg_value=0.5*(S_a_trolley_angle_v_2(i)+S_a_trolley_angle_v_2(i-1));
        S_a_trolley_angle_v_2_i = S_a_trolley_angle_v_2_i+...
           avg_value*abs(w(i-1)-w(i));
        avg_value=0.5*(S_m_trolley_distance_h_2(i)+S_m_trolley_distance_h_2(i-1));
        S_m_trolley_distance_h_2_i = S_m_trolley_distance_h_2_i+...
           avg_value*abs(w(i-1)-w(i));
        avg_value=0.5*(S_v_trolley_distance_h_2(i)+S_v_trolley_distance_h_2(i-1));
        S_v_trolley_distance_h_2_i = S_v_trolley_distance_h_2_i+...
           avg_value*abs(w(i-1)-w(i));
        avg_value=0.5*(S_a_trolley_distance_h_2(i)+S_a_trolley_distance_h_2(i-1));
        S_a_trolley_distance_h_2_i = S_a_trolley_distance_h_2_i+...
           avg_value*abs(w(i-1)-w(i));
        %
        avg_value=0.5*(S_m_trolley_angle_v_twist(i)+S_m_trolley_angle_v_twist(i-1));
        S_m_trolley_angle_v_twist_i = S_m_trolley_angle_v_twist_i+...
           avg_value*abs(w(i-1)-w(i));

avg_value=0.5*(S_m_trolley_angle_v_average(i)+S_m_trolley_angle_v_average(i-1));
        S_m_trolley_angle_v_average_i = S_m_trolley_angle_v_average_i+...
           avg_value*abs(w(i-1)-w(i));
      end
      %
      % RMS values
      %
      RMS_surge_CAPED(ibeta,iHS)= sqrt(S_surge_CAPED_i);
      RMS_surge_RRDF(ibeta,iHS) = sqrt(S_surge_RRDF_i);
      RMS_heave_CAPED(ibeta,iHS)= sqrt(S_heave_CAPED_i);
      RMS_heave_RRDF(ibeta,iHS) = sqrt(S_heave_RRDF_i);
      RMS_sway_CAPED(ibeta,iHS) = sqrt(S_sway_CAPED_i);
      RMS_sway_RRDF(ibeta,iHS)  = sqrt(S_sway_RRDF_i);
      RMS_roll_CAPED(ibeta,iHS) = sqrt(S_roll_CAPED_i);
      RMS_roll_RRDF(ibeta,iHS)  = sqrt(S_roll_RRDF_i);
      RMS_pitch_CAPED(ibeta,iHS)= sqrt(S_pitch_CAPED_i);
      RMS_pitch_RRDF(ibeta,iHS) = sqrt(S_pitch_RRDF_i);
      RMS_yaw_CAPED(ibeta,iHS)  = sqrt(S_yaw_CAPED_i);
      RMS_yaw_RRDF(ibeta,iHS)   = sqrt(S_yaw_RRDF_i);
      RMS_m_t_CAPED_v_1(ibeta,iHS)  = sqrt(S_m_t_CAPED_v_1_i);
      RMS_m_t_CAPED_h_1(ibeta,iHS)  = sqrt(S_m_t_CAPED_h_1_i);
      RMS_v_t_CAPED_v_1(ibeta,iHS)  = sqrt(S_v_t_CAPED_v_1_i);
      RMS_v_t_CAPED_h_1(ibeta,iHS)  = sqrt(S_v_t_CAPED_h_1_i);
      RMS_a_t_CAPED_v_1(ibeta,iHS)  = sqrt(S_a_t_CAPED_v_1_i);
      RMS_a_t_CAPED_h_1(ibeta,iHS)  = sqrt(S_a_t_CAPED_h_1_i);
      RMS_m_t_RRDF_v_1(ibeta,iHS)   = sqrt(S_m_t_RRDF_v_1_i);
      RMS_m_t_RRDF_h_1(ibeta,iHS)   = sqrt(S_m_t_RRDF_h_1_i);
```

```
        RMS_v_t_RRDF_v_1(ibeta,iHS)   = sqrt(S_v_t_RRDF_v_1_i);
        RMS_v_t_RRDF_h_1(ibeta,iHS)   = sqrt(S_v_t_RRDF_h_1_i);
        RMS_a_t_RRDF_v_1(ibeta,iHS)   = sqrt(S_a_t_RRDF_v_1_i);
        RMS_a_t_RRDF_h_1(ibeta,iHS)   = sqrt(S_a_t_RRDF_h_1_i);
        RMS_m_trolley_angle_v_1(ibeta,iHS) = sqrt(S_m_trolley_angle_v_1_i);
        RMS_v_trolley_angle_v_1(ibeta,iHS) = sqrt(S_v_trolley_angle_v_1_i);
        RMS_a_trolley_angle_v_1(ibeta,iHS) = sqrt(S_a_trolley_angle_v_1_i);
        RMS_m_trolley_distance_h_1(ibeta,iHS) = sqrt(S_m_trolley_distance_h_1_i);
        RMS_v_trolley_distance_h_1(ibeta,iHS) = sqrt(S_v_trolley_distance_h_1_i);
        RMS_a_trolley_distance_h_1(ibeta,iHS) = sqrt(S_a_trolley_distance_h_1_i);
        RMS_m_t_CAPED_v_2(ibeta,iHS)  = sqrt(S_m_t_CAPED_v_2_i);
        RMS_m_t_CAPED_h_2(ibeta,iHS)  = sqrt(S_m_t_CAPED_h_2_i);
        RMS_v_t_CAPED_v_2(ibeta,iHS)  = sqrt(S_v_t_CAPED_v_2_i);
        RMS_v_t_CAPED_h_2(ibeta,iHS)  = sqrt(S_v_t_CAPED_h_2_i);
        RMS_a_t_CAPED_v_2(ibeta,iHS)  = sqrt(S_a_t_CAPED_v_2_i);
        RMS_a_t_CAPED_h_2(ibeta,iHS)  = sqrt(S_a_t_CAPED_h_2_i);
        RMS_m_t_RRDF_v_2(ibeta,iHS)   = sqrt(S_m_t_RRDF_v_2_i);
        RMS_m_t_RRDF_h_2(ibeta,iHS)   = sqrt(S_m_t_RRDF_h_2_i);
        RMS_v_t_RRDF_v_2(ibeta,iHS)   = sqrt(S_v_t_RRDF_v_2_i);
        RMS_v_t_RRDF_h_2(ibeta,iHS)   = sqrt(S_v_t_RRDF_h_2_i);
        RMS_a_t_RRDF_v_2(ibeta,iHS)   = sqrt(S_a_t_RRDF_v_2_i);
        RMS_a_t_RRDF_h_2(ibeta,iHS)   = sqrt(S_a_t_RRDF_h_2_i);
        RMS_m_trolley_angle_v_2(ibeta,iHS) = sqrt(S_m_trolley_angle_v_2_i);
        RMS_v_trolley_angle_v_2(ibeta,iHS) = sqrt(S_v_trolley_angle_v_2_i);
        RMS_a_trolley_angle_v_2(ibeta,iHS) = sqrt(S_a_trolley_angle_v_2_i);
        RMS_m_trolley_distance_h_2(ibeta,iHS) = sqrt(S_m_trolley_distance_h_2_i);
        RMS_v_trolley_distance_h_2(ibeta,iHS) = sqrt(S_v_trolley_distance_h_2_i);
        RMS_a_trolley_distance_h_2(ibeta,iHS) = sqrt(S_a_trolley_distance_h_2_i);
        RMS_m_trolley_angle_v_twist(ibeta,iHS) = sqrt(S_m_trolley_angle_v_twist_i);
        RMS_m_trolley_angle_v_average(ibeta,iHS)                                    =
sqrt(S_m_trolley_angle_v_average_i);
    end
end
%
figure(1)
[th,r]=meshgrid((0:beta_incr:360)*pi/180,0.5:0.5:30);
[X,Y]=pol2cart(th,r);
h=polar(th,r);delete(h);
hold on
c_p=[0.0:1.0:25.0];
contour(X',Y',RMS_m_trolley_angle_v_average*180/pi,c_p),caxis([0 25]),colorbar
title('Relative Trolley Angle (deg) - Vertical - Average')
%
figure(2)
[th,r]=meshgrid((0:beta_incr:360)*pi/180,0.5:0.5:30);
[X,Y]=pol2cart(th,r);
```

```
h=polar(th,r);delete(h);
hold on
c_p=[0.0:0.20:5.0];
contour(X',Y',RMS_m_trolley_angle_v_twist*180/pi,c_p),caxis([0 5]),colorbar
title('Relative Trolley Angle (deg) - Vertical - Twist')
```

THIS PAGE INTENTIONALLY LEFT BLANK

LIST OF REFERENCES

1. United States Marine Corps, *MAGTF Planner's Reference Manual* (MAGTF Staff Training Program (MSTP) Pamphlet 5-0.3), Quantico, VA: MSTP Center, MCCDC, pp. 123 – 125, April 2001.

2. United States Marine Corps, MAGTF Deployment Support System II (MDSS II) and Computer Aided Embarkation Management System (CAEMS), database available on CD-ROM—LOG/AIS version 6.3, San Diego, CA: Logistics Training Department Embarkation Division, Expeditionary Warfare Training Group, Pacific, March 2001.

3. Ammunition data was obtained from the U.S. Marine Corps Blount Island Command. POC is MAJ Stefanou (StefanouMS@matcombic.usmc.mil). October 2002

4. Headquarters U.S. Marine Corps, Operational Maneuver From the Sea, Washington, D.C.: Department of the Navy, 1996.

5. Beck & Reed, Modern Computational Methods for Ships in a Seaway, 12 August 2001.

6. WAMIT User manual Versions 6.0, 6.0PC, 5.3S, WAMIT Inc., www.wamit.com, December 2002

THIS PAGE INTENTIONALLY LEFT BLANK

INITIAL DISTRIBUTION LIST

1. Defense Technical Information Center
   Ft. Belvoir, Virginia

2. Dudley Knox Library
   Naval Postgraduate School
   Monterey, California

3. Fotis A. Papoulias
   Naval Postgraduate School
   Monterey, California

4. Brian Higgins
   United States Coast Guard
   Oak Harbor, WA

THIS PAGE INTENTIONALLY LEFT BLANK